Phys. Med. Biol. **53** (2008) R61–R109 doi:10.1088/0031-9155/53/9/R01

**TOPICAL REVIEW**

# The physics, biophysics and technology of photodynamic therapy

**Brian C Wilson**[1] **and Michael S Patterson**[2]

[1] Division of Biophysics and Bioimaging, Ontario Cancer Institute and Department of Medical Biophysics, University of Toronto, 610 University Avenue, Toronto, ON M5G 2M9, Canada
[2] Department of Medical Physics, Juravinski Cancer Centre and Department of Medical Physics and Applied Radiation Sciences, McMaster University, 699 Concession Street, Hamilton, ON L8V 5C2, Canada

E-mail: wilson@uhnres.utoronto.ca and mike.patterson@jcc.hhsc.ca

Received 28 January 2008, in final form 7 March 2008
Published 9 April 2008
Online at stacks.iop.org/PMB/53/R61

**Abstract**

Photodynamic therapy (PDT) uses light-activated drugs to treat diseases ranging from cancer to age-related macular degeneration and antibiotic-resistant infections. This paper reviews the current status of PDT with an emphasis on the contributions of physics, biophysics and technology, and the challenges remaining in the optimization and adoption of this treatment modality. A theme of the review is the complexity of PDT dosimetry due to the dynamic nature of the three essential components—light, photosensitizer and oxygen. Considerable progress has been made in understanding the problem and in developing instruments to measure all three, so that optimization of individual PDT treatments is becoming a feasible target. The final section of the review introduces some new frontiers of research including low dose rate (metronomic) PDT, two-photon PDT, activatable PDT molecular beacons and nanoparticle-based PDT.

## Contents

1. Introduction R62
2. Clinical status R63
   2.1. Cancer R63
   2.2. Localized infection R65
   2.3. Macular degeneration R66
   2.4. Dermatology R66
   2.5. Other clinical indications R67
3. Biological targets in PDT R67
4. Light propagation in tissue R67
   4.1. The transport equation R68

  

4.2. Optical properties of tissues and their measurement R68
4.3. Solving the transport equation R71
4.4. Light fluence distributions in PDT treatments. R72
5. PDT technologies R74
5.1. Light sources R74
5.2. Light delivery technologies R77
5.3. Photosensitizers R81
6. PDT dosimetry R82
6.1. Introduction R82
6.2. Light dosimetry R84
6.3. Photosensitizer dosimetry R84
6.4. Implicit dosimetry R86
6.5. Direct dosimetry R88
6.6. Dose-rate effects R90
6.7. Dosimetry clinical case study: PDT of the prostate R92
6.8. Treatment planning—is PDT dose important? R94
7. Tissue response monitoring R95
8. Emerging developments in PDT R96
8.1. Metronomic PDT R97
8.2. Two-photon PDT R97
8.3. PDT molecular beacons R100
8.4. Nanoparticle-based PDT R101
9. Summary R101
Acknowledgments R102
References R102

## 1. Introduction

Photodynamic therapy (PDT) is the use of drugs (photosensitizers) that are activated by light. In the first step of the process a photosensitizer is administered to the patient, either locally or systemically. After a delay (ranging from minutes to days) to allow for optimum biodistribution, the treatment site is irradiated with visible or near-infrared light. Absorption of this light by the photosensitizer initiates photochemical reactions generating cytotoxic products that result in the desired therapeutic effect.

In 1986, this journal published a review article by the present authors entitled 'The physics of photodynamic therapy' (Wilson and Patterson 1986). This was intended as a status report from a physics/engineering viewpoint and identified a number of outstanding challenges in improving the clinical effectiveness of this novel treatment modality. These included the need for better photosensitizers and for a deeper understanding of the mechanisms of action of PDT, both in cells and *in vivo*. Several limitations in the available light sources and delivery instrumentation for clinical applications were identified and believed to be amenable to engineering solutions. Light dosimetry was at an embryonic stage, with very limited experimental data on the optical scattering and absorption properties of tissues at wavelengths of interest for determining light distributions in tissues for PDT, particularly for human tissues *in vivo*. Only simple models of light propagation were available, with limited accuracy under realistic clinical conditions.

Significant progress has been made in the ensuing two decades, and a primary purpose of this paper is to bring the reader up to date with these advances. At the same time, the field of PDT itself has evolved markedly, so that new challenges have arisen. The following sections

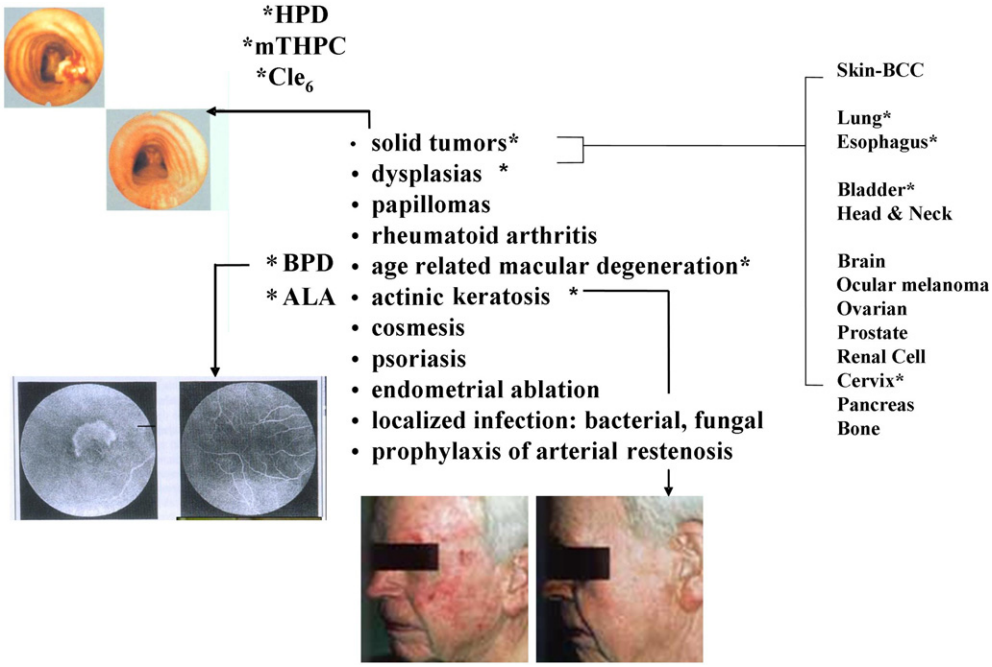


**Figure 1.** Current clinical applications of PDT, showing examples before and after treatment (∗ indicates approved photosensitizer/indication): images show a solid tumor in the upper airway before and 5 years (disease free) after Photofrin (HPD)-PDT; Visudyne-PDT treatment of AMD showing closure of the neovasculature and preservation of the normal retinal vessels; ALA-PDT treatment of actinic keratosis. The list of solid tumor treatments is in roughly descending order of number of clinical trial patients reported.

briefly outline these advances and challenges from the clinical, technological, chemical, biological and physical perspectives. The history of PDT is presented in detail in a recent paper by Moan and Peng (2003), so we will not repeat this here. Rather, we will confine the discussion to the present era, which began with the first substantial animal and human tumor studies by Dougherty and colleagues in the late 1970s (Dougherty *et al* 1978, 1979). It is interesting to note, however, that the first observations of photodynamic effect now are over a hundred years old.

## 2. Clinical status

Figure 1 summarizes the range of clinical applications of PDT, either established (having government approvals) or in active clinical trials. The current status has been presented in detail in recent reviews (Brown *et al* 2004, Maisch 2007, Mennel *et al* 2007). The clinical advantages and potential limitations of PDT are summarized in table 1: these include both generic and application-specific characteristics, as highlighted in more detail below.

### *2.1. Cancer*

The indication for which PDT was initially developed is local destruction of solid tumors. Trials have been performed for tumors of many different sites. The first tumor site approved

**Table 1.** Main advantages and limitations of photodynamic therapy. The limitations are classified as fundamental to the concept or imposed by current technology.

| | Limitations | |
|---|---|---|
| Advantages | Fundamental | Current technology |
| *General* | | |
| Platform technology with wide spectrum of potential applications | Limited light penetration in tissues | No general-purpose light systems |
| Minimally invasive | (Hence) not generally applicable to systemic disease | Limited use and accuracy of patient-specific dosimetry and consequent treatment optimization |
| Low systemic toxicity | | |
| Multiple mechanisms of biological effect | Complex to optimize because of multiple factors | |
| Can be repeated without inducing significant resistance or hypersensitivity | | |
| Highly 'portable' and relatively low-cost technologies | | |
| *Solid tumors* | | |
| Rapid effect in single treatment | Oxygen dependent (for one-photon excitation) | Limited target specificity of clinical photosensitizers |
| Can be curative, palliative or prevent progression | Challenging to achieve adequate treatment throughout larger solid tumor masses | |
| *Age-related macular degeneration* | | |
| Stops or slows disease progression | One-photon excitation may cause collateral damage | Needs to be repeated several times to halt progression |
| *Localized infection* | | |
| Effective against a wide range of micro-organisms, including antibiotic-resistant strains | Not known | Cost of light sources |
| Topically applicable without inducing systemic toxicity or disease resistance | | Delivery of photosensitizer over extended period |

was treatment of refractory superficial bladder cancer (Nseyo *et al* 1998) using Photofrin® as the photosensitizer, with transurethral light delivery to illuminate the whole bladder wall. In this case, the tumor selectivity depends primarily on the selectivity of photosensitizer uptake. Other approvals include treatment of both obstructive and early-stage bronchial cancers (Usuda *et al* 2006), where the light is applied through a bronchoscope and the tumor is either illuminated from the accessible surface or an optical fiber is inserted interstitially. Similar progress has been made in the esophagus, where obstructive lesions are treated for palliation or, at the other end of the tumor progression spectrum, PDT has recently been approved for Barrett's Esophagus patients with high-grade dysplasia as an alternate to esophagectomy to eliminate the risk of the dysplasia proceeding to adenocarcinoma (Overholt *et al* 2007). For skin cancer, PDT has been shown to have high efficacy (Fien and Oseroff 2007), especially for basal cell carcinoma, including extensive (basal cell nevus syndrome) or recurrent lesions. However, its role vis-a-vis other treatments, particularly local excision, has yet to be fully established. Tumors for which PDT has been less effective to date include squamous cell skin tumors that have relatively poor response with the photosensitizers used to date and melanoma

(where the light penetration is a limitation). In malignant brain tumors, there have been several clinical trials of PDT as an adjunctive therapy, including randomized prospective trials in both primary and recurrent tumors. In this case, the whole surgical cavity is illuminated immediately following radical resection in order to reduce the residual tumor burden. There is evidence of strong light dose response dependence, with clinically significant improvements in survival at high doses (Stylli and Kaye 2006). For prostate cancer, clinical trials are in progress at several centers, using multiple interstitial fiber-optic light delivery (see section 6.7) to treat the whole prostate in patients who have recurred locally following radical radiation therapy (Trachtenberg *et al* 2007) or as a primary therapy for focal tumors (Eggener *et al* 2007). In intraperitoneal disseminated ovarian cancer and in mesothelioma, trials have been reported in which an entire body cavity surface is illuminated in an attempt to destroy unresectable disease, with partial success to date (Cengel *et al* 2007). These treatments pose major challenges for generating enough light to treat the very large surface areas and in delivering this adequately to all parts of the complex body space. In head and neck cancer, there have been a number of trials for different problems: widespread and unresectable or recurrent tumors (Biel 2006), early-stage oral cancers (Hopper *et al* 2004) and, most recently, nasopharyngeal tumors for which a special trans-nasal light delivery system has been developed for use with the photosensitizer mTHPC (Nyst *et al* 2007). The early clinical results for the latter are highly positive. A major motivation in these cases is the possibility of avoiding or minimizing mutilating surgery or the complications of high-dose radiotherapy. Hence, it can be seen that PDT has been used at different stages in cancer patient management, including palliation, as a surgical adjuvant, as a stand-alone modality for cure of primary lesions and for prophylactic treatment of dysplasias. Other challenging tumors for which clinical work has been started include biliary tree tumors (using intra-ductal optical fiber light delivery) and pancreatic cancer treated laparoscopically. In addition, there are several new sites that are still in the pre-clinical stages, for example treatment of spinal metastases to debulk tumor mass prior to vertebroplasty for mechanical stabilization (Burch *et al* 2005). Besides solid tumors, PDT has also been investigated (with the photosensitizer merocyanine 540) for purging of tumor and stem cells in bone marrow transplantation, with some success (Miyagi *et al* 2003), although this has not reached the approval stage. The challenge has been to achieve high anti-tumor effect while retaining high survival and patency of normal cells.

### *2.2. Localized infection*

A recent development has been the use of PDT for the treatment of localized bacterial infection. In part this is driven by the rapidly developing problem of antibiotic resistance of many bacterial strains. PDT with a variety of photosensitizers (generally not the same groups of compounds used in oncology) has been shown to be effective against even multi-drug-resistant strains (Demidova and Hamblin 2004, Tang *et al* 2007). PDT with methylene blue has recently been approved in Canada for treatment of periodontitis, in which a gel formulation of the drug is applied to each infected gum pocket and then light is delivered via an optical fiber, also placed into each infected pocket (Wilson 2004). Other ongoing trials include the sterilization of chronic infected wounds (as in, for example, diabetic ulcers) and of the nares (nostrils) to destroy the bacteria that are the major source of peri-operative self-infection of surgical wounds. PDT (with ALA-PpIX, see below) has been tested clinically also as an anti-fungal agent, including *Candida* (Chabrier-Rosello *et al* 2005), and is also used off-label for treatment of acne (Gold 2007), where it kills the associated bacterium *A. vulgaris*. These uses involve application of the drug and the light directly to the infected tissue. Other options are the sterilization of *in situ* implanted devices, such as in-dwelling catheters, and the use of PDT for 'field sterilization', for example of operating room surfaces to prevent the growth of bacteria.

In the 1980s there was also considerable activity in the use of PDT to purge blood of viral agents pre-transfusion, particularly HIV and hepatitis (Ben Hur 1998). While this was technically successful, the economics of the technique were not favorable, and there was concern about re-injection of blood that contained photosensitizer. Nevertheless, reduction of viral levels by several orders of magnitude could be achieved with acceptable toxicity to the normal blood cells, so that this technique may re-emerge with the development of photosensitizers that can be used at lower concentrations and that show high anti-viral activity.

### *2.3. Macular degeneration*

The 'home run' for PDT in the past decade has been in the treatment of age-related macular degeneration (AMD). This is the leading cause of blindness in the elderly in the Western world. The so-called wet form, for which PDT is effective and has been used in over two million cases to date, involves the abnormal growth of blood vessels in the choriocapillaris, possibly in response to chronic hypoxia. These leaky vessels cause loss of central vision. Prior to PDT the only treatment was the use of thermal laser coagulation, but this was marginally effective. In this disease, since the neovasculature is the target, the light is delivered (from a diode laser through a fundus camera) to irradiate typically a 3 mm diameter spot a few minutes after intravenous injection of the photosensitizer Visudyne®, while the drug is still in the vascular compartment. This kills the vascular endothelial cells, resulting in thrombosis and vessel closure (see figure 1). It should be noted that this treatment does not directly restore lost vision, since damage to the photoreceptor layer has invariably occurred by the time treatment is given. However, PDT, which usually requires several rounds of treatment over several months, slows or halts further vision loss (Bressler *et al* 2005). Visudyne-PDT is now the standard treatment of this disease, although a possible alternative has recently been developed in which an anti-angiogenic drug or antibody is injected into the eye. Trials evaluating the combination of PDT and this anti-VEGF therapy are underway.

### *2.4. Dermatology*

As mentioned above, PDT has been tested extensively for skin tumors and is particularly effective in basal cell carcinoma: however, it has not been approved for this indication, largely because the established alternatives (excision, cryosurgery) have very high success rates, so that huge clinical trials would be required to demonstrate improved efficacy. It has been shown in trials to be particularly useful for basal cell nevus syndrome, which involves large areas of multiple lesions, and for treatment of difficult sites, such as on the eyelids, where the excellent healing due to preservation of the tissue collagen is a significant advantage.

Most dermatological PDT now uses ALA-PpIX as the photosensitizer (Nestor *et al* 2006). In this, the photosensitizer protoporphyrin IX (PpIX) is synthesized endogenously in the target cells as part of the heme biosynthesis pathway after administration of the pro-drug 5-aminolevulinic acid (ALA). ALA-PDT is an approved therapy for actinic keratosis or sun-damaged skin (Tschen *et al* 2006), which often occurs on the face and scalp and is associated with development of skin cancer. In this case the ALA is applied topically and short wavelength (blue) light is used to minimize the depth of treatment, since the disease is very superficial. This approval has led to widespread, off-label use of topical ALA-PDT in cosmetic dermatology, e.g. in treatment of acne, in hair removal (the treatment damages the hair follicles) and in skin re-modeling.

PDT has also been evaluated for treatment of psoriasis (Smits *et al* 2006), a common condition where there is uncontrolled proliferation of keratinocytes, leading to formation of

'plaques', that are particularly debilitating on joints such as the elbows and knees. Other forms of phototherapy, either UV-B treatment or PUVA (in which UV-A is used to activate the drug 8-methoxypsoralen, which intercalates into DNA and prevents cell division upon photoactivation), are also options for psoriasis, but are associated with a risk of UV-induced skin cancer. Hence, PDT using visible light-activated photosensitizers is an attractive option (in this case the treatment causes direct cell death rather than reducing proliferation) but its efficacy for psoriasis is not yet established.

### *2.5. Other clinical indications*

There are several other clinical applications for which PDT has been investigated using a variety of photosensitizers, including rheumatoid arthritis, with light delivered by optical fibers into the inflamed joints or, more recently, transdermally for small joints (Funke *et al* 2006) and for preventing restenosis of arteries following angioplasty for artherosclerotic plaque (Chou *et al* 2002), in which the light is administered via an intravascular optical fiber.

## 3. Biological targets in PDT

In the case where mammalian tissues are the target, the clinical effect can be due to direct target cell death (e.g. tumor cells) by necrosis or apoptosis, vascular damage leading to tissue ischemia and resultant target cell death, or immune modulation, or a combination of these. One of the potential advantages of PDT is that the choice of photosensitizer and the other treatment parameters, such as the drug-light time interval, the total PDT 'dose' and the light fluence rate can, at least in part, be adjusted to select the primary biological targets and resulting responses (Henderson *et al* 2006). For example, treatment of AMD deliberately exploits the vascular response, while bone marrow purging is purely cellular. Tumor treatments often involve a combination of these biological targets and responses.

Unlike radiation therapy, DNA is not the major target (typically photosensitizers localize in/on cell membranes, frequently mitochondrial membranes) and the cell death is somatic (i.e. the treated cells themselves die) rather than anti-proliferative (Gomer *et al* 1996). As a result, tissue responses are very rapid and sometimes detectable even before treatment has been completed. Since PDT is usually given as a single, high dose rather than extended over many fractions, there is little opportunity for adjustment of the treatment parameters. Combined with the fact that the tissue responses can be quite heterogeneous (both within a target volume and between targets or patients), this means that pre-treatment optimization can be critical. However, since the responses are rapid and marked, there is the possibility of using on-line monitoring of the tissue response (e.g. altered blood flow, the presence of a necrotic treatment 'boundary', etc) to compensate for under-dosing of the target and to avoid over-dosing of adjacent normal tissues, see section 7. In addition, PDT can be repeated multiple times, as has been done in the case of skin tumors, without apparent induction of resistance (presumably since DNA is not targeted and so there is no opportunity for treatment-induced mutation or selection) or of exceeding tissue tolerance (since there is preservation of the collagen (Barr *et al* 1987) and, hence, of the tissue architecture).

## 4. Light propagation in tissue

Before describing the current technical status of PDT it is useful to discuss the physics of light propagation in tissue (optically turbid media) and mathematical models that are useful for its description. The optical properties of tissue and their measurement will also be summarized.

### 4.1. The transport equation

In our original review paper (Wilson and Patterson 1986), we described the radiation transport equation (RTE) and the necessary interaction coefficients. Here, we briefly update that discussion to use currently recommended nomenclature and symbols (Hetzel *et al* 2005). For simplicity we assume that the light is monoenergetic (monochromatic), but the extension to a broad spectrum is straightforward (ignoring inelastic scattering and fluorescence). The fundamental quantity in the RTE is the energy radiance, $L(\mathbf{r}, \mathbf{\Omega})$, defined as the radiant power transported at location $\mathbf{r}$ in a given direction $\mathbf{\Omega}$ per unit solid angle per unit area perpendicular to that direction. The SI unit is W m$^{-2}$ sr$^{-1}$. A photosensitizer molecule in tissue can be excited by light traveling in any direction, so that the integral of the radiance over $4\pi$ solid angle controls the rate of photochemical activation. This quantity is called the energy fluence rate, $E_0(\mathbf{r})$. Note that the SI units of the energy fluence rate are W m$^{-2}$ and it is important that this quantity not be confused with the irradiance, which has the same units and is defined as the radiant power incident on an infinitesimal surface element divided by the area of that element. The irradiance is defined only for a particular surface, whereas the fluence rate can be defined and measured in free space or within a tissue volume. To complete the RTE for the energy radiance we must also specify the linear absorption coefficient, $\mu_a$, and differential scattering coefficient, $\mu_s(\mathbf{\Omega}' \rightarrow \mathbf{\Omega})$, where $\mathbf{\Omega}'$ and $\mathbf{\Omega}$ are the propagation directions before and after elastic scattering. Integration of the differential scattering coefficient over all final directions yields the total scattering coefficient, $\mu_s$. In general, all the interaction coefficients can be functions of position, so the final time-dependent RTE looks like

$$\frac{1}{v}\frac{\partial}{\partial t}L(\mathbf{r}, \mathbf{\Omega}, t) + \mathbf{\Omega} \cdot \nabla L(\mathbf{r}, \mathbf{\Omega}, t) + [\mu_a(\mathbf{r}) + \mu_s(\mathbf{r})]L(\mathbf{r}, \mathbf{\Omega}, t) = \int_{4\pi} L(\mathbf{r}, \mathbf{\Omega}', t)\mu_s(\mathbf{r}, \mathbf{\Omega}' \rightarrow \mathbf{\Omega})\ \mathrm{d}\mathbf{\Omega}' + S(\mathbf{r}, \mathbf{\Omega}, t) \tag{1}$$

where $v$ is the speed of light in the tissue. Note that this equation also includes a source term, $S(\mathbf{r}, \mathbf{\Omega}, t)$, representing either internal light sources (such as implanted optical fibers) or the distribution of first-scatter events from an external source such as a collimated laser beam. Boundary conditions for the radiance are generally required as well.

Exact solution of equation (1) is possible under only a few conditions, and in practical cases various approximations must be employed. As the validity of these depends on the optical properties of the medium, we first consider the absorption and scattering coefficients of tissues in the wavelength range used for PDT. Typically this is 600–800 nm, although shorter wavelengths in the blue and green are occasionally employed in treating very superficial disease.

### 4.2. Optical properties of tissues and their measurement

The absorption coefficient of tissue is determined by the concentration of light-absorbing molecules (chromophores). This relation can be expressed as

$$\mu_a = \sum_k C_k \sigma_k \tag{2}$$

where $C_k$ is the molecular concentration of chromophore $k$ and $\sigma_k$ is its molecular absorption cross-section. (This can also be expressed as the product of the molar concentration and the molar extinction coefficient, as is commonly done in the photochemistry literature.) At PDT wavelengths the two most important chromophores are hemoglobin and water, although in some cases lipids, melanin and other pigments such as bilurubin can also make significant

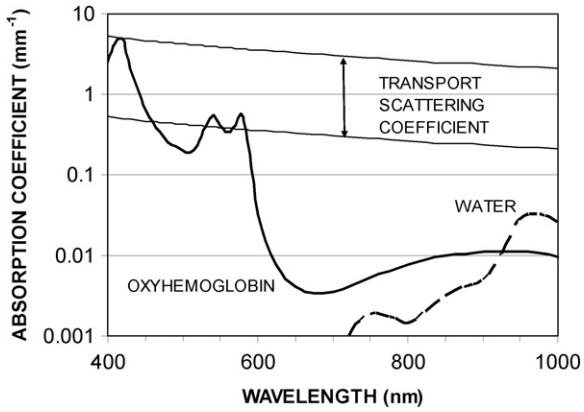


**Figure 2.** The absorption coefficients of the two most important tissue chromophores in the PDT spectral range are plotted versus wavelength for concentrations typical of soft tissue: 40 $\mu$M for oxy-hemoglobin and 40 M for water. The approximate range for reported values of the transport scattering coefficient is also indicated.

contributions. The absorption cross-section of hemoglobin changes when oxygen binds to the protein (oxy-hemoglobin). In figure 2, the product $C{\cdot}\sigma$ has been plotted as a function of wavelength for oxy-hemoglobin and water for typical soft tissue concentrations of 40 $\mu$M and 40 M, respectively.

The scattering coefficient of tissue is much more difficult to estimate. While the scattering of isolated dielectric particles is well understood, the complex architecture of tissue results in variations in the index of refraction on many different length scales. Some success has been achieved with fractal models (Schmitt and Kumar 1998, Sheppard 2007, Xu and Alfano 2005) that incorporate this structure, but most of our knowledge is based on experiment. The angular dependence of the differential scattering coefficient, also referred to as the phase function, can be measured directly using a goniometer and thin (tens of microns) tissue slices (Firbank *et al* 1993, Flock *et al* 1987, Ghosh *et al* 2001, Key *et al* 1991). An elegant microscope-based system that allows the measurement of scattering from a small tissue volume has also been described by Popp *et al* (2003). These results (see figure 3) show that scattering in tissue is peaked in the forward direction, with the average cosine of the scattering angle (the anisotropy factor, $g$) >0.9. By using slices of different thicknesses and a narrow beam geometry, the total attenuation coefficient, $\mu_t = \mu_s + \mu_a$, can also be determined (Firbank *et al* 1993, Flock *et al* 1987, Ghosh *et al* 2001, Key *et al* 1991). Typical results are 10–50 mm$^{-1}$, indicating that the mean free path between elastic scattering events is the order of a few cell diameters. Because the scattering is forward-peaked, several scattering events are necessary to completely randomize the direction of light propagation. Hence, it is useful to think of an effective isotropic or reduced scattering coefficient, given by $\mu_s' = (1 - g)\mu_s$. The range of reported values for this parameter, also referred to as the transport scattering coefficient, is indicated in figure 2. Note that this is typically one or two orders of magnitude larger than the absorption coefficient in the PDT spectral range.

In our original review (Wilson and Patterson 1986), we summarized the existing data on tissue optical properties. A major review has been published since then (Cheong *et al* 1990), but the data are still relatively sparse. A major impediment to the acquisition of a comprehensive data set has been the difficulty of performing suitable measurements, particularly *in vivo*. The characterization of excised tissue samples is somewhat easier but subject to errors due to preparation and handling artifacts, such as freezing/thawing and blood drainage. As described

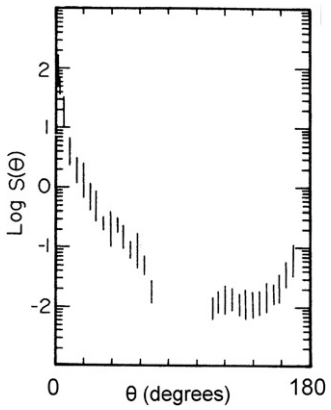


**Figure 3.** Scattering phase function measured *ex vivo* for porcine brain tissue at 633 nm (Flock *et al* 1987). Vertical bars represent the range of values obtained for three 20 $\mu$m tissue slices. The average cosine of the scattering angle is 0.94.

above, the differential scattering coefficient can be reliably measured for thin (optically single scattering) samples. At PDT wavelengths a narrow beam measurement of $\mu_t$ is essentially a measure of the total scattering coefficient, since $\mu_s \gg \mu_a$. However, solution of the RTE requires knowledge of $\mu_s$, $\mu_a$ and $g$. Determining $\mu_a$ directly is difficult for thin (i.e. one mean free path) samples, because the probability of absorption is so small. Hence, thick samples must be used, but then multiple scattering must be accounted for.

A typical setup (Beek *et al* 1997, Peters *et al* 1990, Pickering *et al* 1993, Simpson *et al* 1998) for measuring the optical properties of an optically thick tissue sample is shown in figure 4. A collimated beam of the desired wavelength is incident on the sample and two integrating spheres serve to collect the diffusely transmitted and reflected light that has been multiply scattered in the tissue. Clearly, there is no simple relation between the diffuse reflectance, $R$, or diffuse transmittance, $T$, and the fundamental interaction coefficients defined above. Instead, a model of light propagation and detection must be used iteratively to improve estimates of the interaction coefficients, so that measured and calculated results for $R$ and $T$ are in best agreement. This method has been used successfully to estimate $\mu_a$ and $\mu_s'$ but it is not sensitive to differences in $g$ or $\mu_s$ as long as the product $(1 - g)\,\mu_s$ is conserved. In order to estimate all three parameters, a supplementary narrow-beam or thin-sample experiment is necessary. Obviously, measurements such as those in figure 4 must be performed for optically-homogeneous samples of a single tissue type to obtain meaningful results.

When measurements are attempted *in vivo*, it is rarely possible to confine the light to tissue of one type, especially when non-invasive methods are used. To date the main approach used in PDT, at least for solid tumors, has been to implant fiber-optic sources and detectors within the organ of interest and to measure the resulting light distributions, as will be discussed below (see sections 6.2 and 6.7). In that case, a model of light propagation in a homogeneous medium can be used to deduce the interaction coefficients from a set of internal measurements, e.g. the fluence rate at two distances from an internal source of known power.

A more general, non-invasive approach is depicted in figure 5. In this, multiple sources and detectors are placed on the external boundary of a heterogeneous tissue volume. The geometry and identity of the constituent tissue types can be provided by MRI or CT, using image segmentation, and the goal is to estimate the optical interaction coefficients of each tissue type. Significant progress has been made in solving this problem, which is the basis for

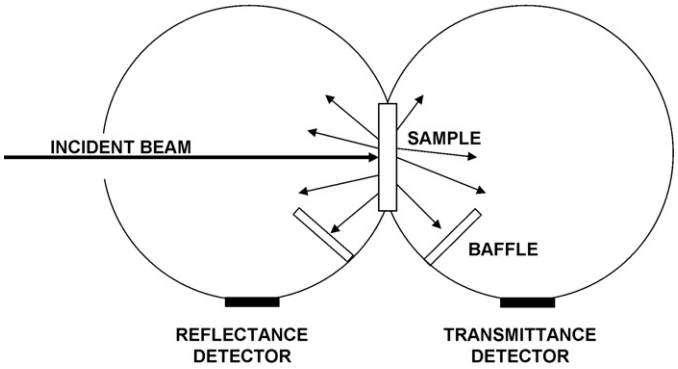


**Figure 4.** Typical apparatus for the measurement of the optical properties of tissue samples *ex vivo*. The sample is illuminated by a collimated beam, and the diffuse reflectance and transmittance are detected via the two integrating spheres. The baffles block direct light paths from the sample to the detectors.

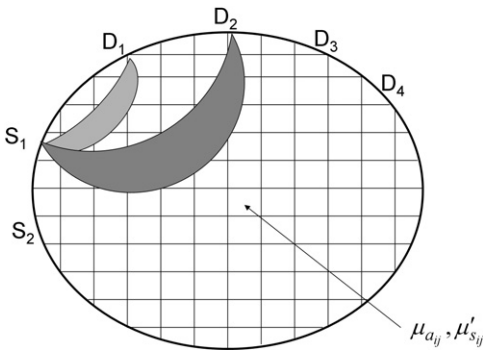


**Figure 5.** Schematic diagram showing the general arrangement for the measurement of the optical properties *in vivo*. The goal is to estimate the absorption and scattering coefficients of each voxel from measurements of light transmission between source–detector pairs. These measurements may be continuous wave (cw), time domain, or frequency domain. Because of multiple scattering, light may follow any path from a source to a given detector, but some trajectories are more probable than others. The shaded 'bananas' from $S_1$ to $D_1$ and $D_2$ encompass the paths of highest probability. The source–detector geometry and the detection scheme can be modified so that certain voxels are preferentially investigated. *A priori* information about tissue morphology can also be used to group pixels of the same tissue type and reduce the degrees of freedom in this generally ill-posed problem.

diffuse optical tomography (Gibson *et al* 2005), by iteratively improving the estimates of the optical interaction coefficients at each voxel so that the calculated and measured data agree. Both steady-state and time-resolved (or equivalent frequency-domain) measurements can be performed (Delpy *et al* 1988). A key part of the process is a forward solution of the RTE that can yield rapid solutions for a heterogeneous medium. Such solutions will be discussed below.

### *4.3. Solving the transport equation*

Once the optical properties of the tissue are known, the RTE can be used to calculate the fluence rate at any position for a given source specification. For almost all cases of interest in

PDT an analytic solution of the RTE is not possible, so that approximate methods are needed. The three different approaches were described in some detail in our original review paper (Wilson and Patterson 1986), so here we will focus on the advantages and limitations of each. The simplest and most widely used approach is to replace the RTE with a diffusion equation for the fluence rate, $E_0(\mathbf{r})$,

$$\frac{1}{v}\frac{\partial}{\partial t}E_0(\mathbf{r},t) - \nabla \cdot \frac{1}{3(1-g(\mathbf{r}))\mu_s(\mathbf{r})}\nabla E_0(\mathbf{r},t) + \mu_a(\mathbf{r})E_0(\mathbf{r},t) = S(\mathbf{r},t). \tag{3}$$

This approximation requires that the radiance is almost isotropic or, more precisely, that it can be expressed as the sum of only two terms: one independent of and the other proportional to the cosine of propagation direction. Generally, this condition is met if $\mu_a < 0.1\mu_s'$ and if the point of interest is far from sources or boundaries. In optically-homogeneous tissue, analytic solutions of equation (3) exist for many useful cases, such as a point source in an infinite medium, a broad (effectively infinite) beam incident on a semi-infinite medium and a line source in an infinite medium (Jacques 1998). If the optical properties are position dependent, a variety of numerical methods can be used. The most widely adopted is the finite-element method (Arridge *et al* 1993, 2000, Pogue *et al* 2001), for which public domain or commercial software is available. Provided the conditions for using the diffusion equation are met, many studies have shown that the fluence rate can be calculated to about 10% accuracy or better. If higher accuracy is required, or if there are doubts about the validity of the diffusion approximation, a more accurate method of solving the RTE must be employed.

Monte Carlo modeling, widely used in ionizing radiation dosimetry (Rogers 2006), is one such method. In this case the fluence is estimated from the number of photon interactions scored in each volume element, and the accuracy of the estimate depends on the number of photon histories tracked in the simulation. Position-dependent optical interaction coefficients can be incorporated, although the programming overhead to support this may be considerable. A free, widely used Monte Carlo code for light propagation in tissue is available (Wang *et al* 1995). As simulations usually require millions of photon histories, Monte Carlo is not often used for routine calculations. Typically, it is most useful for generating exact solutions (within the stochastic limits) that can be used to check the accuracy of more rapid calculation methods.

The third approach is a numerical solution of the RTE, which falls into two subclasses (Patterson *et al* 1990a). In the discrete ordinates method the direction and (if necessary) position variables are discretized and the system of equations thereby generated from the RTE is solved numerically to estimate the radiance and hence the fluence rate. In the second subclass the radiance is expressed as the sum of basis functions, such as the spherical harmonics. The RTE is then replaced by a system of equations, one for each of the harmonics retained in the series. (The diffusion equation can be regarded as the lowest-order solution.) In infinite media, the computationally efficient modified spherical harmonics algorithm has been applied to PDT problems (Markel 2004, Xu and Patterson 2006). In either subclass, it may be necessary to solve a large system of equations if the radiance is highly anisotropic.

### *4.4. Light fluence distributions in PDT treatments.*

As discussed in section 5.2, there are several different 'geometries' for light irradiation in PDT. From the perspective of the physics of light propagation in tissue, these may be grouped into surface and interstitial irradiation. Surface irradiation includes cases where the light source is external to the body (e.g. treatment of skin lesions) or is placed within and illuminates the inner surface of a body cavity (e.g. a hollow organ or a surgical resection space). Interstitial treatments are usually done by placing an optical fiber that carries the light directly into the tissue. Here, we will summarize for each case the main features of the resulting spatial

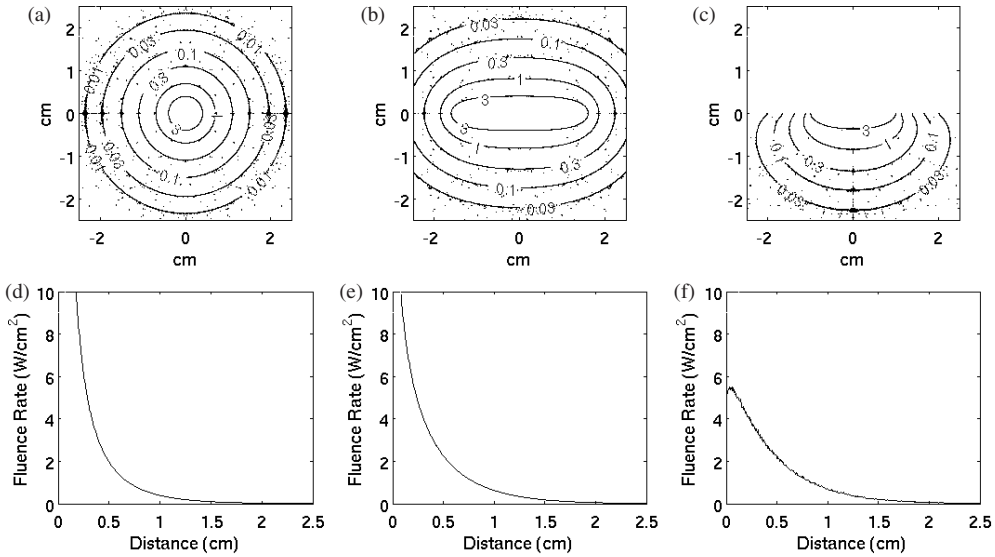


**Figure 6.** Typical fluence rate distributions during PDT. These were calculated using Monte Carlo simulations assuming $\mu_a = 0.01$ mm$^{-1}$, $\mu_s = 10$ mm$^{-1}$, $g = 0.9$ and tissue index of refraction $= 1.4$. (a) Isofluence rate lines for a 1 W point source; (d) corresponding plot of fluence rate versus distance from the source; (b) isofluence rate lines for a 3 cm cylindrical source emitting 1 W cm$^{-1}$; (e) corresponding plot of fluence rate versus radial distance from the center of the source; (c) isofluence rate lines for a 2 cm diameter beam normally incident on the tissue surface with irradiance 1 W cm$^{-2}$; (f) corresponding plot of fluence rate versus depth along the central axis of the beam. Note that the fluence rate just below the tissue surface is more than five times the incident irradiance. About 60% of the incident light is lost by diffuse reflectance.

distribution of the light, which depends on the optical properties as discussed above. We will assume that the tissue is optically homogeneous, i.e. that the absorption and scattering are constant within the treatment volume, and that the tissue volume is large compared to the typical light propagation distances. We also assume that the scattering is much larger than the absorption, which is true for most tissues at typical PDT wavelengths above about 630 nm.

*4.4.1. Surface irradiation.* Figure 6 shows the distribution of the fluence rate for a broad-beam surface irradiation. Unlike the absorption-dominated case (Beer's law), the 'depth dose' is not a simple single-exponential form, but shows a sub-surface peak and only becomes exponential at some depth beyond this. Mathematically,

$$E_0(z) = EB(z)\ \exp(-\mu_{\text{eff}} z) \tag{4}$$

where $E$ is the surface irradiance, $B$ is a backscatter factor and the so-called effective attenuation coefficient

$$\mu_{\text{eff}} = \sqrt{3\mu_a \mu_s'}. \tag{5}$$

$B(z)$ depends in a complex way on the tissue absorption and scattering coefficients at the treatment wavelength and on the tissue surface (air or liquid coupling): in general, it increases with beam size and can be up to about 5. The effective penetration depth is given by $\delta = 1/\mu_{\text{eff}}$. This is the incremental depth in tissue over which the fluence rate falls to $1/e$ of its previous value. The penetration depth is not equal to the depth of PDT treatment, $d_t$, since this depends

on the photosensitizer concentration, tissue oxygenation, intrinsic tissue photosensitivity and total light dose. Typically, for most clinical photosensitizers, $d_t \sim 3$–$5\delta$.

The loss of backscattered light through the tissue surface (diffuse reflectance) can be greater than 50% at long wavelengths for lightly pigmented tissues. This represents a loss of therapeutic light to the target volume. Conversely, in the case of closed cavity irradiation, most or all of this light re-enters the tissue, increasing the actual fluence rate compared to the delivered (primary) irradiance. This increase can be as high as 5–7 times in bladder or esophagus (Star *et al* 1987). The depth distribution also gets steeper, so that the dose is more superficial. The backscatter factor may be highly variable from patient to patient: in the bladder, for example, this can lead to increased normal tissue damage if the delivered light dose is not adjusted to take it into account.

The lateral spreading of the light from scattering increases the effective beam diameter by typically a few mm, which may be important clinically if there are adjacent critical normal tissues. If the beam diameter is small ($<\sim 5\delta$), the fluence rate at depth will be reduced for the same irradiance, since there is a reduced volume of tissue for scatter into the beam.

*4.4.2. Interstitial irradiation.* For interstitial treatments, geometric spreading of the light causes an additional decrease in the fluence rate with radial distance, $r$, from the source. For a point isotropic source emitting power $P$

$$E_0(r) \approx \frac{3P\mu_s'}{4\pi r} \exp(-\mu_{\text{eff}} r) \tag{6}$$

For a cylindrical diffusing fiber (see section 5.2) the dependence on $r$ is more complex and depends on the diffuser length, but qualitatively the behavior is similar. The shape of the distribution at each end of a diffusing fiber is roughly the same as for a point source, but there is no simple algebraic expression to describe it. The resulting distributions are illustrated in figure 6.

In practice, clinical target volumes are neither optically completely homogeneous nor unbounded, so that the theoretical distributions above can be significantly distorted. In addition, $\mu_a$ may change during treatment due to changes in blood flow caused by the vascular PDT response, and this can alter the fluence distribution. This effect is less marked above about 650 nm, where the hemoglobin absorption is less, but is more pronounced for vascularly-acting photosensitizers. A further complication is that the molar extinction coefficients of some photosensitizers can be very high, so that the added absorption due to the photosensitizer itself can be significant compared to the intrinsic tissue absorption, and so can decrease the penetration depth.

## 5. PDT technologies

Clinical advances have both driven and been enabled by the development of technologies for PDT. This involves the photosensitizers themselves (discussed in the next section) and a variety of 'hardware', including light sources, light delivery systems and technique and instruments for PDT dosimetry.

### *5.1. Light sources*

The basic requirements for PDT light sources (Brancaleon and Moseley 2002) are to match the activation spectrum of the photosensitizer (usually the longest wavelength peak) and to generate adequate power at this wavelength, deliverable to the target tissue ergonomically

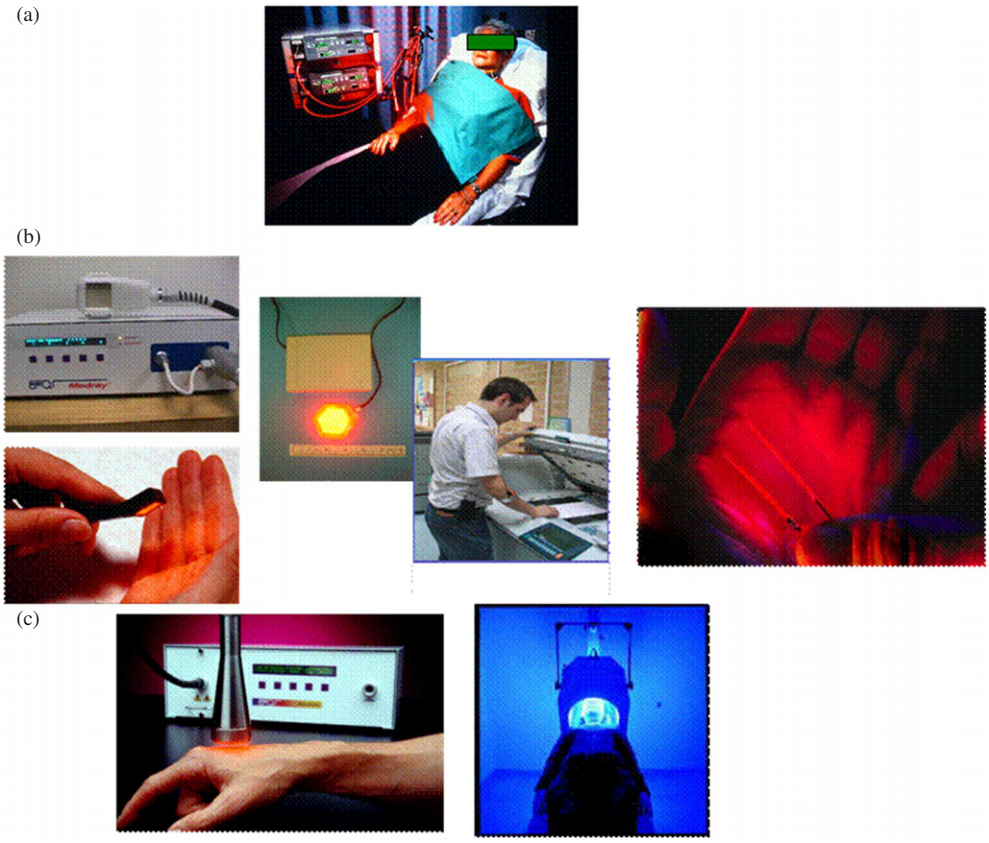


**Figure 7.** Examples of light sources for clinical PDT. (a) Diode lasers with fiber-optic light delivery (*Miravant*, *USA*); (b) LEDs showing (left) planar array including power/control box (*EXFO*, *Canada*) and a miniature planar array for intra-oral use (*PRP Optoelctronics*, *UK*), (center) LED and power pack for mobile use (Moseley *et al* 2006, *reproduced with permission from Blackwell Synergy*), (right) linear arrays for interstitial use (*Light Sciences*, *USA*); (c) filtered lamps (left) arc lamp with light guide delivery (*EXFO*, *Canada*) and (right) fluorescent lamps in a U form used for ALA-PpIX skin treatments (*DUSA*, *USA*).

and with high efficiency. Typically, 1–5 W of usable power are required in the 630–850 nm range at irradiances of up to several hundred mW $cm^{-2}$ in order to deliver treatments in tens of minutes. In addition, the sources must be reliable in the clinical environment and be cost-effective.

Examples of the three main classes of clinical PDT light source—lasers, LEDs and filtered lamps—are shown in figure 7. In the late 1970s/early 1980s, most clinical treatments were performed with an argon-ion laser (∼5–10 W) pumping a dye laser. While generating adequate power and having the advantage of wavelength tunability so that the same source could be used for different photosensitizers, this technology is not well suited to the clinical environment because of size, electrical power and water-cooling requirements, and poor reliability. A significant advance in the 1980s was to replace the argon-ion laser by an all-solid-state frequency-doubled Nd:YAG (KTP) laser source, which solved some of the reliability and cooling issues but was still cumbersome and expensive. KTP-dye systems have been largely superseded by diode lasers, which are now the standard source for many PDT applications. The main advantages of lasers are (a) the high efficiency (>90%) of coupling into single optical

fibers for endoscopic and interstitial light delivery (see below) and (b) their monochromaticity, which gives maximum efficiency of photoactivation. The main limitation of diode lasers, which are otherwise very convenient and reliable, is that they are single-wavelength devices, so that a separate unit is required for each photosensitizer.

Light emitting diodes have become a viable technology for PDT in the past few years, particularly for irradiation of easily accessible tissue surfaces. The main advantages over (diode) laser sources is the low cost and ease of configuring arrays of LEDs into different irradiation geometries. Output power used to be a limitation, but now LED arrays with hundreds of mW $cm^{-2}$ are available spanning most of the visible–NIR spectrum. Linear arrays of LEDs have been developed that can be used endoscopically or even interstitially. The main limitation, particularly for the latter, remains the relatively poor electrical-to-light conversion efficiency of conventional LEDs ($<\sim$15%), which means generated heat must be removed. Coupling of single LEDs into single optical fibers has recently been demonstrated with efficiencies of about 50% and 25% into 600 $\mu$m and 350 $\mu$m core fibers respectively (Davies 2006), at least at low power, so that LED-fiber source-delivery packages may become an option in the near future for some applications. As with laser diodes, LEDs have fixed output wavelength, but the cost per watt is significantly less, so that having different sources for each photosensitizer is less of a drawback.

A number of lamp systems available for PDT have the advantage that they can be spectrally filtered to match any photosensitizer. However, they can be efficiently coupled only into optical fiber bundles or liquid light guides ($\sim$5–10 mm diameter), so that endoscopic use is not possible. As with LEDs, flexible geometry is an advantage, as shown by the example of the U-shaped filtered fluorescent tube arrays used for blue-light irradiation of the whole face and scalp for actinic keratosis (figure 7).

With broadband sources the effective output power is reduced compared with a laser source at the photosensitizer activation peak and is proportional to the integrated product of the source output spectrum and the photosensitizer activation spectrum. For LEDs and filtered lamps the output spectrum typically has a bandwidth of about 25–30 nm, so that the efficiency factor for typical photosensitizer spectra (also $\sim$tens of nm bandwidth) is about 50%.

Potential light source developments in the near-to-mid term future include

- multi-wavelength laser diode systems, as illustrated in figure 8, in which 'plug-in modules' would allow the wavelength to be changed without having to completely replicate the complete power and control system,
- LED arrays with user-configurable geometry to match to the treatment area,
- novel light source technologies, such as organic LEDs, or chemiluminescence-based sources, for example in the form of 'light patches' (Zelickson *et al* 2005).

Among the major technological challenges are

- reducing the cost of sources, particularly diode lasers that are typically $\sim$\$50 K for 2–3 W units (the modular system above would contribute to this),
- low-cost systems for community or even home-care use, particularly for treating localized infections,
- extending this concept to the development of disposable packages with integrated light source and delivery components,
- light sources for extended, low-power treatments (metronomic PDT, see section 8.1) and
- Ultrafast (fs) pulsed laser sources for two-photon PDT (also discussed below in section 8.2).

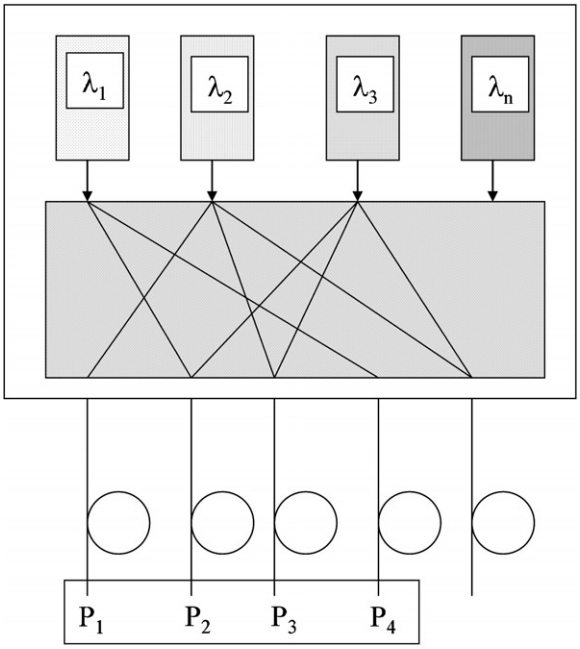


**Figure 8.** Concept of a modular, multi-wavelength diode laser system for PDT allowing selection of the wavelength to match several different photosensitizers, using a common power and control platform. This has not yet been produced commercially.

### *5.2. Light delivery technologies*

Given the wide range of clinical applications of PDT and the many different body sites, there has been considerable development in the past 20 years of means to deliver the light from the source to the target tissue. Unlike ionizing radiation, it is not feasible to deliver adequate power to the target tissue through the overlying normal tissues, because of the high scattering and consequent limited penetration of visible/NIR photons. Hence, there is high reliance on fiber-optic technology.

Examples of light delivery for specific treatment sites are shown in figure 9. In surface irradiation, depending on accessibility of the treated surface, the light may be used directly from the source with no delivery system, via a lens system (e.g. the fundus camera in AMD, figure 9(e)), via a fiber bundle/light guide (in the use of filtered lamps) or via a single fiber-optic (e.g. placed through the instrument channel of an endoscope) with or without a microlens tip to give a flat rather than Gaussian output beam profile. For intracavitary treatments, a means to disperse the light isotropically from the fiber is required. For approximately spherical cavities, such as the resection cavity after surgical debulking of brain tumors or the urinary bladder, this can be achieved either (a) by filling the cavity with a light-scattering medium, usually the lipoprotein colloid Intralipid (van Staveren *et al* 1991), which has very low red–NIR absorption and so minimizes attenuation or (b) by incorporating a light-scattering tip on the end of the fiber (van Staveren *et al* 1995). Particularly in case (a), care has to be taken to avoid blood leakage into the cavity, since this can result in significant light loss. An alternative to filling the cavity itself with Intralipid is to use an inflatable balloon applicator (figures 9(c) and (d)). These can also be shaped to match more irregular body cavities and the balloon material itself can be made light scattering instead of filing it with a light-scattering liquid or a diffusing-tip

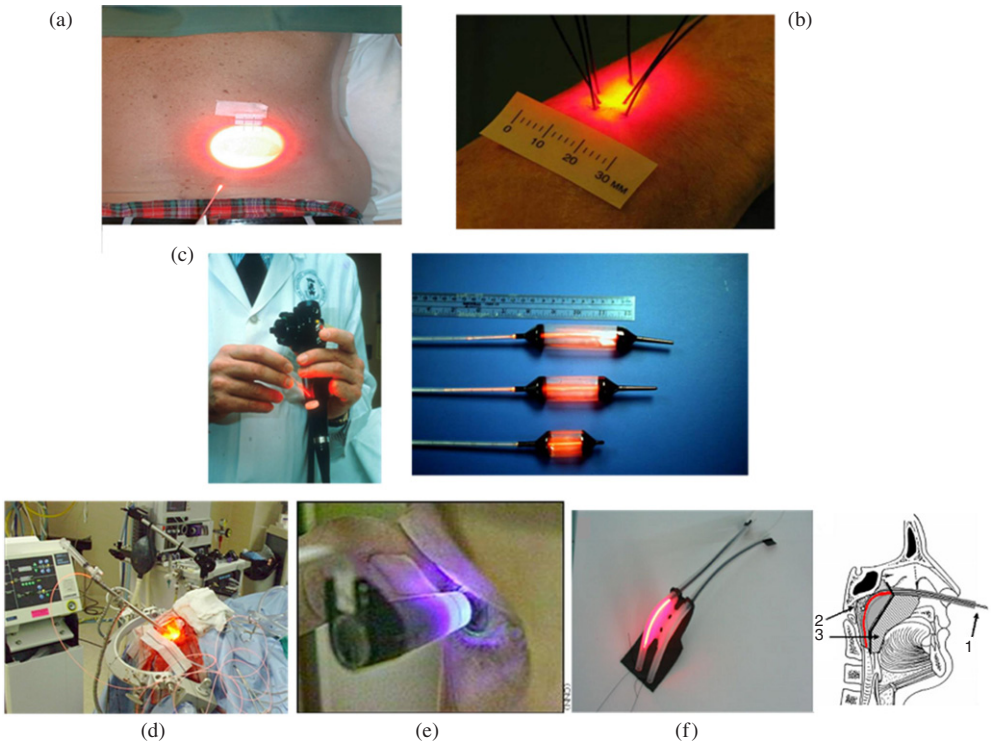


**Figure 9.** Light applicators for clinical PDT: (a) surface and (b) interstitial irradiation using optical fibers (*courtesy S Andersson-Engels*), (c) placement of linear diffuser fiber into endoscope instrument channel (left) and balloon applicators for endoscopic esophageal PDT (*courtesy N. Marcon*), (d) intracavitary irradiation of brain tumor surgical resection bed using a balloon filled with Intralipid to scatter uniformly the light delivered from a KTP-dye laser (on left) by an optical fiber, (e) transcorneal delivery to treat AMD, (f) nasopharyngeal applicator (after Nyst *et al* 2007, *reproduced with permission from Wiley Interscience*).

fiber may be used within the balloon. A recent development (figure 9(f)) has been the use of a light diffusion device specifically designed for treatment of nasopharyngeal tumors (Nyst *et al* 2007).

For interstitial treatments, rather than using a fiber with a simple cleaved tip, a cylindrically-diffusing fiber is often used so that each fiber irradiates a larger volume of tissue. The commercially available fibers (e.g. those manufactured by Medlight, Lausanne, Switzerland) are made by stripping the cladding and coating the fiber core with a light-scattering material along the desired length of the diffusing tip. Diffusers with good uniformity (typically $\pm 15\%$) are available for lengths up to 5–10 cm, with outside tip diameters around 1 mm. Multiple diffusing fibers can be used (simultaneously or sequentially) to irradiate larger/deeper tissue volumes, and an example is given in figure 10 of this approach for PDT of prostate cancer where the objective is to treat the whole gland. The spacing of the fibers is then set by the tissue optical properties in order to achieve the required uniformity of light dose.

A recent development has been the fabrication of diffusing fibers that are deliberately non-uniform along their length (Rendon *et al* 2006). An example is shown in figure 11 that is designed to provide an output profile such that there is a constant fluence along the boundary of the prostate (assuming specific tissue optical properties and tissue PDT sensitivity). Rather

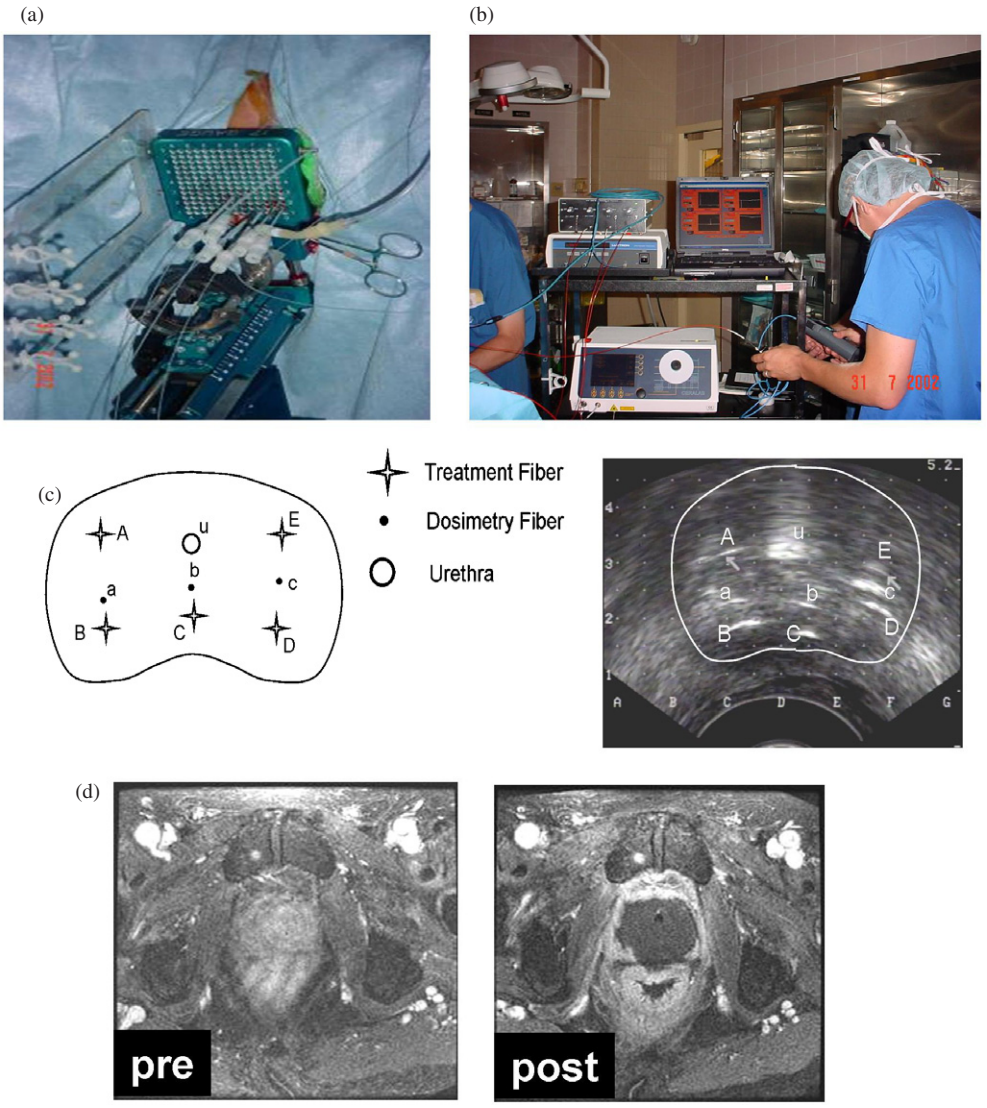


**Figure 10.** Multi-fiber interstitial PDT of whole prostate for locally-recurrent cancer after radical radiation therapy. (a) Multiple source and detector fibers placed into the prostate through a brachytherapy template under transrectal ultrasound guidance; (b) diode laser source (lower shelf) and multi-channel light dosimetry system (upper) in use during treatment; (c) reconstruction of the fiber placement superimposed on the transverse ultrasound image; (d) gadolinium contrast-enhanced MRI of the prostate prior to and at 7 days following vascularly-targeted PDT (*courtesy M Haider and J Trachtenberg*).

than coating the fiber with a light-scattering material, a Bragg grating is written into the fiber tip by exposing the photoreactive core to a specific pattern of UV light, thereby changing the refractive index (figure 12(a)). Such fibers are used commonly in telecommunications for multiplexing, since they transmit only selected wavelengths. As PDT diffusers (Vesselov *et al* 2005), the refractive index variations cause scattering of the light out of the core, and it is possible to design the grating pattern so that the required axial output profile is obtained

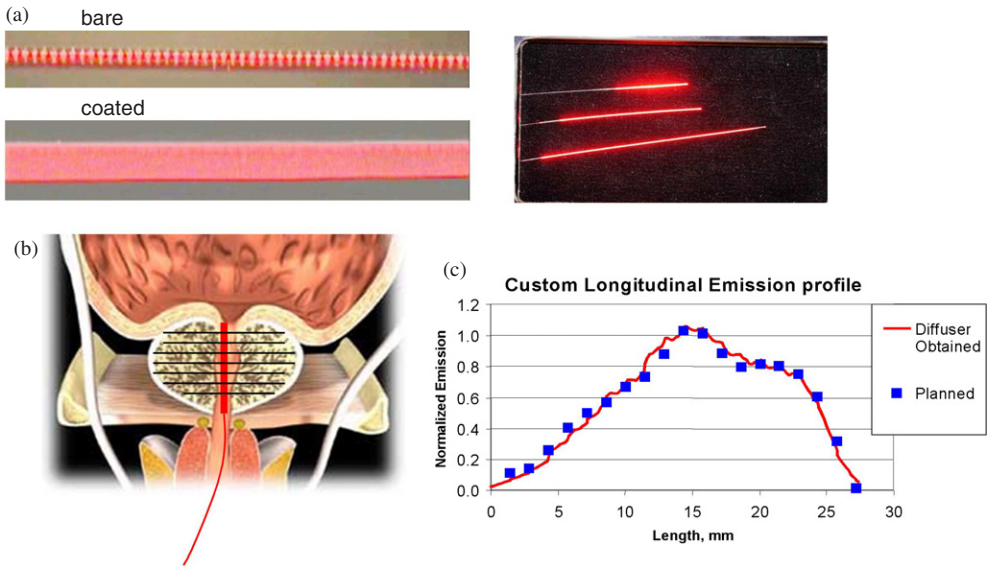


**Figure 11.** Bragg grating fibers for PDT light delivery. (a) The grating written into the fiber core before and after coating and different lengths of coated fiber (uniform grating in these example); ((b) and (c)) longitudinal light output profile designed to match the varying diameter of the prostate comparing the specified distribution determined by inverse treatment planning and the measured distribution (*courtesy L Lilge and colleagues*).

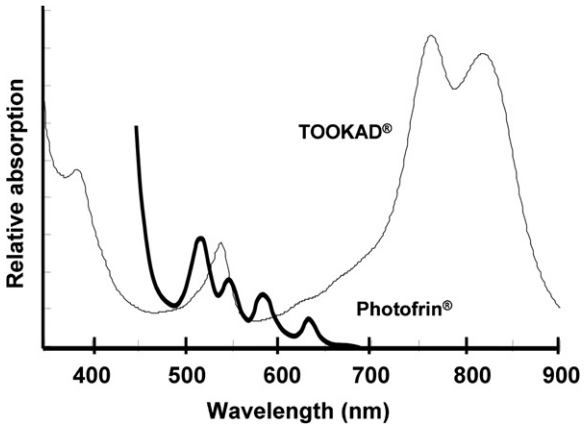


**Figure 12.** Absorption spectra of Photofrin (*Axcan Pharma*, *Canada*), the first sensitizer approved for clinical PDT, and TOOKAD (*Steba-Negma*, *France*) a 'second generation' sensitizer with much higher absorption in the near infrared where light penetration in tissue is maximized.

(figures 11(b) and (c)). An advantage of these fibers is that, being single mode, they also have very small diameters (<200 $\mu$m), so that they are minimally invasive for interstitial or intravascular use. However, this poses a challenge for efficient coupling of diode lasers, which generally do not have a very good $TM_{00}$ output mode. This is, however, a solvable problem, using special coupling lenses.

### 5.3. Photosensitizers

The archetypal photosensitizer is Photofrin® (Axcan, Quebec, Canada), a complex mixture of many different porphyrin molecules derived from blood. Its absorption spectrum is shown in figure 12: like many such molecules, Photofrin has a large 'Soret' band around 400 nm and several smaller 'Q-band' peaks at longer wavelengths. Photofrin has a long residence time in the body, resulting in skin photosensitivity for several weeks. A second limitation is that its longest absorption peak is only at 630 nm, where the penetration of light through tissues is still fairly poor, due to hemoglobin absorption. This peak is also of low cross-section, which increases the drug dose required to achieve adequate photodynamic effect. Despite these limitations, Photofrin has been used widely in the clinic and is often the 'reference' photosensitizer against which others are compared. In general, the 'ideal' PDT agent would have the following properties:

*Photophysical.* High absorption (molar extinction coefficient, $cm^{-1}\,M^{-1}$) at long wavelengths, in the range ~700–850 nm, for maximum light penetration in tissue.

*Photochemical.* High singlet oxygen quantum yield for high photodynamic efficiency but should also be fluorescent to facilitate monitoring its biodistribution by point spectroscopy or imaging; low photobleaching to retain efficacy during treatment or, alternatively, rapid photobleaching so that the treatment becomes self-limiting.

*Chemical.* High stability; single, pure molecular species; ease and low cost of synthesis; water soluble to allow systemic administration without requiring a delivery vehicle such as liposomes or emulsions.

*Biological.* Low dark toxicity; pharmacokinetics matched to the application (e.g. rapid clearance for vascular targeting); selective uptake in target tissues/tissue structures; microlocalization to sensitive cellular/subcellular targets (e.g. mitochondria).

Inevitably, practical photosensitizers involve compromises between these properties. To illustrate this, we will consider other representative second generation sensitizers. The first, TOOKAD (WST09: Steba-Negma, Paris, France) is a bacteriopheophorbide where the Mn ion present in such naturally-occurring molecules in bacteria has been replaced by Pd, thereby giving a very high singlet oxygen quantum yield and high absorption at around 763 nm (figure 12), where $\delta$ in typical soft tissues is around 4 mm (about twice that at 630 nm). The molecule is essentially non-fluorescent, so that its concentration in tissue *in vivo* has to be measured by absorption (diffuse reflectance) spectroscopy, as discussed in section 6.3. It is very rapidly cleared (20 min serum half-life), so that it must be activated within a few minutes of administration, at which time it is still in the vasculature, which is then the biological target. It is not water soluble, so that it is administered in cremophore. A water-soluble analog has recently been reported (Mazor *et al* 2005).

As a second example, many photosensitizers being investigated for anti-infective PDT have very different molecular structures and biophysical properties. Methylene Blue is a particularly simple, small molecule example. Unlike photosensitizers targeted against mammalian cells, the challenge with anti-infective PDT is to destroy microorganisms such as bacteria by damaging the thick cells' walls, the structure and biochemical composition of which are very different between $Gram^+$ and $Gram^-$ species (Jori and Brown 2004). The polarity of the photosensitizer is important in determining its penetration into the bacterial cell wall. In the case of MB-PDT for periodontitis (mentioned above), and for many other anti-infective uses, the photosensitizer is administered topically and so does not have to be water soluble.

## 6. PDT dosimetry

### *6.1. Introduction*

In this section we will address the dosimetry problem, namely, what physical properties should be measured or calculated to predict the biological effect of a PDT treatment? Ancillary questions are: how accurately must these properties be determined and how can they be measured in the clinical environment? These questions can be appreciated better by comparison with ionizing radiation therapy. A century of clinical experience has determined that the biological response is very well correlated with the energy absorbed per unit mass of tissue. The biological response, e.g. probability of tumor control or normal tissue complication rate, is generally a sigmoidal function of this dose and, in the region of steepest gradient, dose changes of 5% can lead to differences in clinical outcomes (van Dyk 1999). Protocols for measuring radiation dose distributions in water or plastic phantoms are well established and form the basis of software packages to calculate the 3D dose distributions in individual patients. Allowance must be made for dose rate and fractionation, and there is still some individual variation in response, but a map of radiation dose is now an indispensable part of almost all ionizing radiation treatments.

The contrast to PDT is striking—in PDT there is no widely accepted definition of dose nor is there agreement on how it should be measured or used to predict response. In part, this can be attributed to the relatively immature state of clinical PDT and the resources that have been invested in its development. However, PDT dosimetry is also inherently a more difficult problem: its complexity arises from the basic mechanism of PDT illustrated in figure 13. Upon absorption of a photon of the appropriate energy the photosensitizer molecule is raised from its ground state ($S_0$) to an electronic excited state ($S_1$). The molecule may return to its ground state via the emission of a photon (indicated as fluorescence in figure 13) but efficient photosensitizers undergo rearrangement of electronic spin to generate a triplet excited state ($T_1$), by inter-system crossing (ISC). The triplet state has a relatively long lifetime in tissue, typically tens of microseconds and, under well-oxygenated conditions, de-excites by energy transfer (ET) to ground-state molecular oxygen, also a triplet state ($^3O_2$). If sufficient energy is provided by this transfer, a singlet excited state of oxygen ($^1O_2$) can be produced with high efficiency—typical sensitizers yield about one molecule of singlet oxygen for every two photons absorbed (Redmond and Gamlin 1999). Considerable evidence now exists that singlet oxygen is the principal mediator of biological damage in PDT (Niedre *et al* 2002, Weishaupt *et al* 1976) but pathways that yield other reactive species are also possible (Foote 1991). A number of studies indicate that tissue necrosis requires the production of $10^{18}$–$10^{19}$ molecules $cm^{-3}$ of singlet oxygen (Farrell *et al* 1998).

The common approach to clinical dosimetry is to measure the photosensitizer administered to the patient (mg $kg^{-1}$) and the incident exposure (product of irradiance and treatment time). There are several reasons why this simplistic solution may be inadequate. First, the local concentration of photosensitizer will vary from site to site in the body, from individual to individual, and as a function of time. Second, the penetration of light into the target tissue will depend on its specific optical properties. Third, if the tissue is hypoxic or becomes hypoxic as a result of the PDT treatment, the yield of singlet oxygen will be lower than expected. To complicate matters further, sensitizer concentration, light penetration and tissue oxygenation can change during treatment and one parameter can influence the other. For example, photochemical reactions can degrade the ground-state sensitizer and loss of its optical absorption can result in greater light penetration. Clearly, a successful strategy for PDT dosimetry must account for these factors.

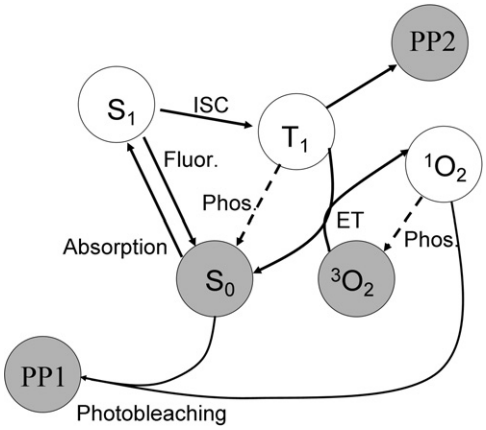


**Figure 13.** Schematic diagram of the basic photophysical processes in PDT. After absorption of a photon, the ground-state sensitizer ($S_0$) is raised to the $S_1$ excited electronic state. This can return to the ground state via emission of light (Fluor.) or undergo a rearrangement of electronic spin (ISC, inter-system crossing) to yield the excited triplet ($T_1$). The triplet transfers energy (ET) to ground-state molecular oxygen producing excited singlet oxygen ($^1O_2$), the reactive species primarily responsible for biological damage. Both singlet oxygen and the sensitizer triplet can emit light (Phos.) via 'forbidden' transitions. Singlet oxygen can react with the ground-state sensitizer molecule which led to its production or, if the concentration is high enough, a different sensitizer molecule to produce a photoproduct (PP1). Other pathways, such as the triplet-mediated mechanism shown here, can also lead to photobleaching and other photoproducts (PP2).

If the biological response is correlated with the amount of singlet oxygen generated, three possible approaches to the dosimetry problem are apparent (Wilson *et al* 1997):

(a) Direct dosimetry, in which singlet oxygen is measured.
(b) Explicit dosimetry, in which the three critical ingredients—light, photosensitizer and oxygen—are measured (ideally continuously) and the singlet oxygen amount is then calculated by knowledge of the relevant reaction pathways. In the simplest case, this quantity is proportional to the product of local photosensitizer concentration and light fluence.
(c) Implicit dosimetry, in which a surrogate for singlet oxygen generation is measured. One strategy is illustrated in figure 13, where $^1O_2$ reacts with ground-state photosensitizer to yield a photoproduct (PP1). If this product, or the photobleaching of the sensitizer, can be monitored, then an implicit measure of singlet oxygen production is possible.

In the following sections we will examine each of these. Section 6.2 will cover light fluence dosimetry and section 6.3 will describe methods for determining the concentration of photosensitizers in tissue. These first two sections are essential components of the explicit dosimetry approach. We will not touch on the measurement of tissue oxygenation as this has been covered in other recent reviews (Buerk 2004, Papkovsky 2004). In section 6.4 the use of implicit measures for singlet oxygen is covered, and direct measurement of singlet oxygen constitutes section 6.5. As in ionizing radiation therapy, the time dependence of the delivered radiation can have a profound effect on the treatment outcome and the basis for this dependence in PDT is outlined in section 6.6. Finally, in section 6.7 we will return to the question of treatment planning and in section 6.8 comment on the importance and required accuracy of PDT dosimetry.

### 6.2. *Light dosimetry*

In section 4.3, we described how the light fluence (rate) can be calculated if the irradiation conditions and tissue optical properties are known. An alternative is to measure the fluence rate directly. This can be done only at discrete points, so that the use of such measurements is similar to the use of *in vivo* point dosimeters in ionizing radiation therapy. The goal is usually to provide experimental support for the calculation of the fluence rate or to measure the fluence rate directly at locations that are clinically critical or where there is low confidence in the calculation (e.g. near boundaries). The measurement is most often made using optical fibers modified so that they collect light over a large solid angle. This can be accomplished by fixing a small amount of light-scattering material at the tip of the fiber (van Staveren *et al* 1995) and coupling the other end of the fiber to a light detector such as a photodiode. Such fiber probes are commercially available with an angular response that varies by only $\pm 5\%$ (except in the backwards direction where the scattering tip is shadowed by the fiber itself). The calibration of such isotropic detectors is itself challenging, since the response is different in air and in tissue because of the mismatch in index of refraction at the surface of the scattering material (Marijnissen and Star 1996, Marijnissen and Star 2002, van Staveren *et al* 1995). An accuracy of about 5–10% in absolute fluence rate measurements can be achieved with these detectors. The outer diameter of the fiber is typically 200 $\mu$m so that they can easily be implanted in tissue. A caveat in the interstitial use of such detectors is that blood pooling at the fiber tip may alter the local fluence rate.

### 6.3. *Photosensitizer dosimetry*

Once the light fluence rate has been determined, the next step in the explicit dosimetry approach is to measure the photosensitizer concentration in the target tissue. The ideal method would be non-invasive and provide a 3D dynamic map of concentration. One approach would be label the photosensitizer with a detectable tracer. Positron emission tomography has been used with radiolabeled sensitizers (Jeeves *et al* 1985, Pandey *et al* 2005, Wilson and Vanlier 1989), but the image resolution is only comparable to the penetration depth of the light and the positron emission is insensitive to photobleaching that affects the concentration of active sensitizer. Most radiological imaging methods are also difficult to perform during the PDT treatment. Optical methods based on fluorescence, absorption or Raman scattering are more compatible with PDT delivery and can provide essentially continuous measurements of concentration. As described below, these techniques usually give the concentration at the point of measurement or the average concentration over some tissue volume rather than a comprehensive map.

As indicated in figure 13, most photosensitizers are fluorescent, typically with a quantum yield of a few per cent. The emission from a small volume of tissue is proportional to concentration, although this relationship may depend on the local chemical environment of the sensitizer, e.g. a change in pH may affect the emission spectrum and the fluorescence quantum yield. Another problem is that the excitation light may have to propagate some distance in tissue before reaching the fluorophore and, similarly, the emission light may have to propagate through tissue to the fluorescence detector. Hence, the detected fluorescence also depends on the tissue optical properties and this effect can be significant. However, if the propagation distance can be reduced, the dependence on the optical properties can be minimized, for example, by delivering the excitation light and collecting the fluorescence emission through the same optical fiber, placed on or into the tissue, as illustrated in figure 14 (Diamond *et al* 2003b). If the fiber core diameter is $<200$ $\mu$m, the error in concentration due to tissue scattering and absorption is less than 10% over a wide range of optical properties (Diamond *et al* 2003b).

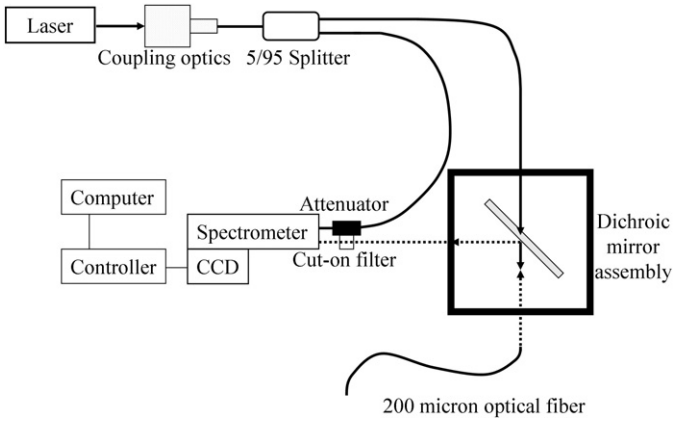


**Figure 14.** Fluorescence measurement system using a single optical fiber for excitation and detection. The fiber may be placed in contact with the tissue surface or inserted interstitially via a hollow needle. If the fiber core is 200 $\mu$m or less, the dependence of the fluorescence signal on the optical properties of the tissue is reduced to less than 10% under typical conditions (Diamond *et al* 2003b).

A limitation of this approach is that the tissue volume sampled is only about 1 $\mu$l and it may be preferable to measure the average sensitizer concentration over the entire target volume. Pogue and Burke (1998) have described a surface probe consisting of a bundle of fibers, each acting independently as source and detector. This effectively samples a much larger tissue volume and also increases the detected signal. Another way to accomplish this is to deliver and collect the light by separate optical fibers some distance apart and to correct for the tissue optical properties. This correction can be empirical or based on mathematical models of light propagation (Diamond *et al* 2003a).

For sensitizers that are non-fluorescent or have very low quantum yield, absorption spectroscopy can be used and has the advantage that the absorption spectrum is less sensitive to changes in the local microenvironment. Referring to equation (2), the goal is to determine the concentration of the sensitizer by determining its specific contribution to the total absorption coefficient. In general, this is most accurate if the absorption coefficient is determined over a range of wavelengths so that characteristic sensitizer peaks can be discriminated from the endogenous tissue background absorption. Figure 15 illustrates a system designed to perform absorption spectroscopy *in vivo* (Farrell *et al* 1994). A probe in contact with the tissue contains a single source fiber and multiple detector fibers at distances of 1–10 mm from the source. White light is delivered to the source fiber and the diffusely reflected light collected by the detector fibers is spectrally resolved by a diffraction grating and charge coupled device (CCD) detector. Note that the CCD simultaneously acquires spatially- and spectrally-resolved information. The reflectance *versus* distance data at each wavelength are fitted by the diffusion model for an optically-homogeneous, semi-infinite medium to estimate $\mu_a$ (total) and $\mu_s'$. Figure 15 (Weersink *et al* 1997) shows an *in vivo* example in skin after injection of the photosensitizer $AlPcS_4$. While the characteristic photosensitizer absorption peak at 670 nm is apparent, the estimated concentration is about one third of the true concentration measured in skin samples *ex vivo*. There is also an obvious artifactual peak in the scattering spectrum. These errors occurred even though very good fits to the reflectance data were obtained. The causes are the layered structure of the tissue and the non-uniform distribution of the sensitizer: the subcutaneous fat layer has low scattering and absorption compared to the skin and a much lower concentration of $AlPcS_4$. These two factors combine to mimic a uniform medium with

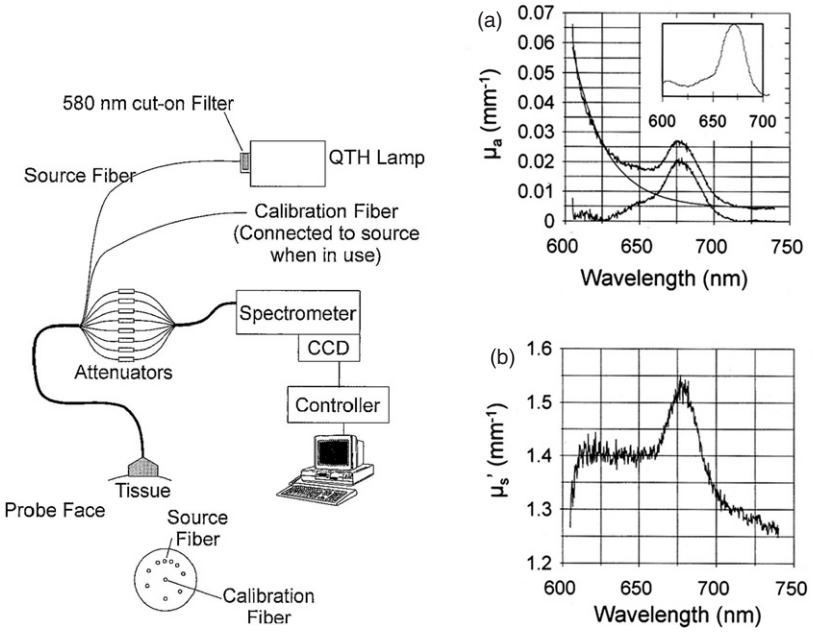


**Figure 15.** A specific example of the general approach outlined in figure 5. The goal is to perform quantitative absorption spectroscopy to estimate the photosensitizer concentration. In this case cw transmission measurements are made simultaneously at many wavelengths between a source fiber and ten detectors at different distances. A diffusion model of light propagation is used to estimate the absorption and scattering coefficients at each wavelength using the assumption that the tissue is homogeneous. The absorption coefficient (graph (a)) shows the characteristic peak of the sensitizer ($AlPCS_4$, see the inset) superimposed on the tissue background. When this background is stripped (bottom curve), the photosensitizer spectrum resembles that measured for the drug in solution, but the amplitude is lower than that expected from independent measurements of drug concentration. The peak in the scattering spectrum (graph (b)) at 680 nm is an obvious artifact. Both of these effects can be attributed to the layered structure of skin and the non-uniform distribution of the sensitizer. *Reproduced from Weersink et al (1997) with permission from Blackwell Synergy.*

the properties shown in figure 15. In principle, this problem could be overcome by using a multilayer model of light propagation but this requires additional information on the tissue structure and absolute reflectance data (Alexandrakis *et al* 1998).

Absorption spectroscopy can also be used to quantify oxy- and deoxy-hemoglobin in tissue (Conover *et al* 2000), and the oxygen saturation, which is linked to the tissue oxygen content (Finlay and Foster 2004). Hence, it is possible to gain information about the third component of explicit dosimetry. This information, however, is obtained over a relatively large tissue volume and may not be sensitive to localized regions of hypoxia on the scale of inter-capillary spacing.

Finally, inelastic (Raman) light scattering has been used to measure the sensitizer concentration in tissue *ex vivo* (Synytsya *et al* 2004) and fiber-optic-based Raman systems developed for *in vivo* diagnostic purposes could be applied to this problem. The main advantage is the high specificity of the Raman molecular signatures.

### *6.4. Implicit dosimetry*

From the preceding section it is clear that measurement and interpretation of all the components of explicit dosimetry is a challenging problem. Nonetheless, this approach has been successful

in some applications and is still being developed (Patterson *et al* 1990b, Zhu *et al* 2005). By contrast, implicit dosimetry seeks a surrogate measure that combines or integrates these separate dose factors. Here, we focus on detection of photobleaching and photoproducts, as illustrated in figure 13. The utility of this approach depends on whether other reactions that are not dependent on singlet oxygen can also cause the same effect—in figure 13 an example of one such pathway, photobleaching via reaction of the sensitizer triplet state is illustrated (Finlay *et al* 2004).

Ignoring such competing processes for the moment, the photobleaching of the sensitizer ground state by reaction with singlet oxygen is a bimolecular reaction (figure 13):

$$S_0 + {}^1O_2 \rightarrow \text{PP1}. \tag{7}$$

If the reaction rate is governed by diffusion we would expect

$$\frac{d}{dt}[S_0] = -k_{os}[S_0][{}^1O_2] \tag{8}$$

where $k_{os}$ is the rate constant. However, Dysart and Patterson (2005) have shown that it may be necessary to take into account the fact that singlet oxygen is generated in close proximity to the photosensitizer molecules. Thus, there is a finite probability, independent of the sensitizer concentration, that it will react with the sensitizer molecule from which it was generated. Equation (8) can be modified by adding a term $\gamma$ that represents an effective minimum sensitizer concentration:

$$\frac{d}{dt}[S_0] = -k_{os}([S_0] + \gamma)[{}^1O_2]. \tag{9}$$

Rearranging equation (9) to solve for $[{}^1O_2]$ and integrating over time gives the following expression for the total amount (or dose) of singlet oxygen generated during a PDT treatment that starts at $t = 0$ and ends at $t = T$:

$$\text{Dose} = \frac{1}{\tau_\Delta}\int_0^T [{}^1O_2]\,dt = \frac{1}{\tau_\Delta k_{os}}\log_e\frac{[S_0]_{t=0} + \gamma}{[S_0]_{t=T} + \gamma} \tag{10}$$

where $\tau_\Delta$ is the singlet oxygen lifetime in the tissue. Note that this equation is valid even if the fluence rate and ambient oxygen concentration change during the treatment. In contrast to explicit dosimetry, all that is required to calculate the absolute dose is a measure of initial and final sensitizer concentrations, $[S_0]_{t=0}$ and $[S_0]_{t=T}$, and knowledge of the parameters $\gamma$, $\tau_\Delta$ and $k_{os}$.

To date this model has been tested only in simple biological systems, such as cell suspensions and multicell spheroids. Dysart and Patterson (2005) varied the fluence rate, sensitizer concentration and oxygenation during PDT of tumor cells with the sensitizer *meta*-tetra(hydroxyphenyl)chlorine (mTHPC) and showed that cell survival was correlated with the dose as calculated by equation (10), see figure 16. Similar experiments with Photofrin (Dysart and Patterson 2005) and ALA-PpIX (Dysart and Patterson 2006) showed that these sensitizers could be photobleached by non-$^1O_2$ pathways under hypoxic conditions, so that it is not possible to apply equation (7) in this situation. Finlay *et al* (2004) came to similar conclusions when they examined the bleaching of Photofrin in multicell tumor spheroids, postulating two different bleaching mechanisms, one mediated by singlet oxygen and the other by the sensitizer triplet state, and that the relative importance of each depends on the ambient oxygen concentration.

This group also suggested that the fluorescent photoproduct of Photofrin is produced only by singlet-oxygen-mediated bleaching, so that a measurement of the concentration of the photoproduct would be more reliable than measuring the photobleaching of Photofrin itself. In their cell suspension system Dysart and Patterson (2005) did not find this difference

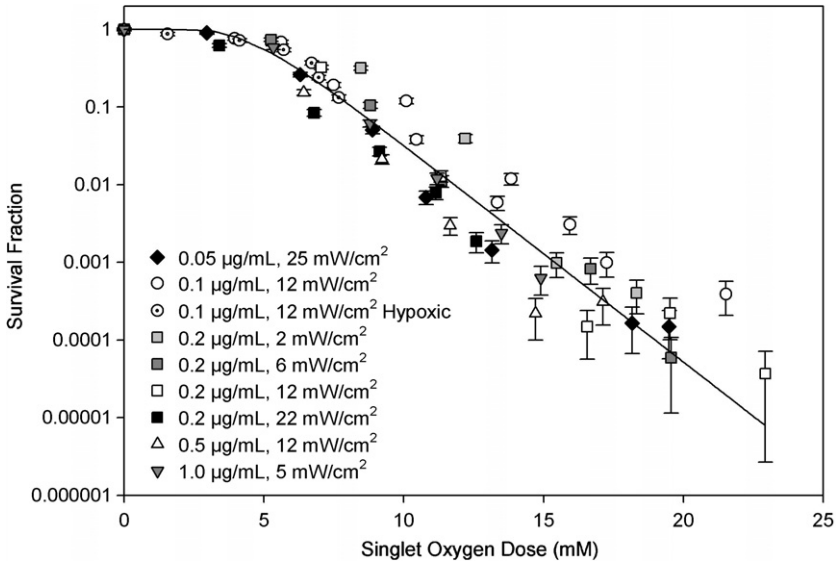


**Figure 16.** MLL cell survival *in vitro* following mTHPC-PDT versus singlet oxygen dose calculated using photobleaching and equation (10). In order to express the dose in absolute terms, measured values of $\gamma$, $k_{os}$ and $\tau_{\Delta}$ were used. Even though PDT was performed under a variety of mTHPC concentrations, fluence rates and oxygenation, cell survival can be predicted from photobleaching.

in the Photofrin photoproduct yield, but did find that the yield of one of the photoproducts of PpIX was correlated with cell survival for ALA-PDT (Dysart and Patterson 2006). Zeng *et al* (2002) demonstrated that the concentration of a photoproduct of benzoporphyrin derivative (BPD) was the most reliable predictor of the PDT response in mouse skin *in vivo*. Another interesting hypothesis put forward by Forrer *et al* (1995) is that the photobleaching of endogenous fluorophores could be used as an indicator of biological damage. Although this autofluorescence bleaching could be measured in patients, it could not be correlated with eventual clinical outcome.

In conclusion, implicit dosimetry is appealing but much more work needs to be done, especially *in vivo*, to establish validity for specific photosensitizers and to demonstrate the links between the implicit dose and relevant biological outcomes. A significant step in this direction is provided by two recent papers that examined the photobleaching of ALA-PpIX during PDT of the rat esophagus (Boere *et al* 2006, Sheng *et al* 2004). Both studies concluded that an initial rapid bleaching phase was correlated with a more effective PDT treatment.

### *6.5. Direct dosimetry*

Given that singlet oxygen has been implicated as the principal cytotoxic molecule in PDT since 1976 (Weishaupt *et al* 1976), it is not surprising that its direct measurement *in vivo* has received considerable attention. The history and state-of-the-art have been reviewed recently by Jarvi *et al* (2006). The basis for direct dosimetry is detection of the weak phosphorescence emitted at 1270 nm when singlet oxygen returns to the ground state via a classically forbidden transition. The amount of light emitted per unit time is directly proportional to the instantaneous concentration of singlet oxygen and the relative probability of this de-excitation pathway. Detection of singlet oxygen luminescence is a standard technique

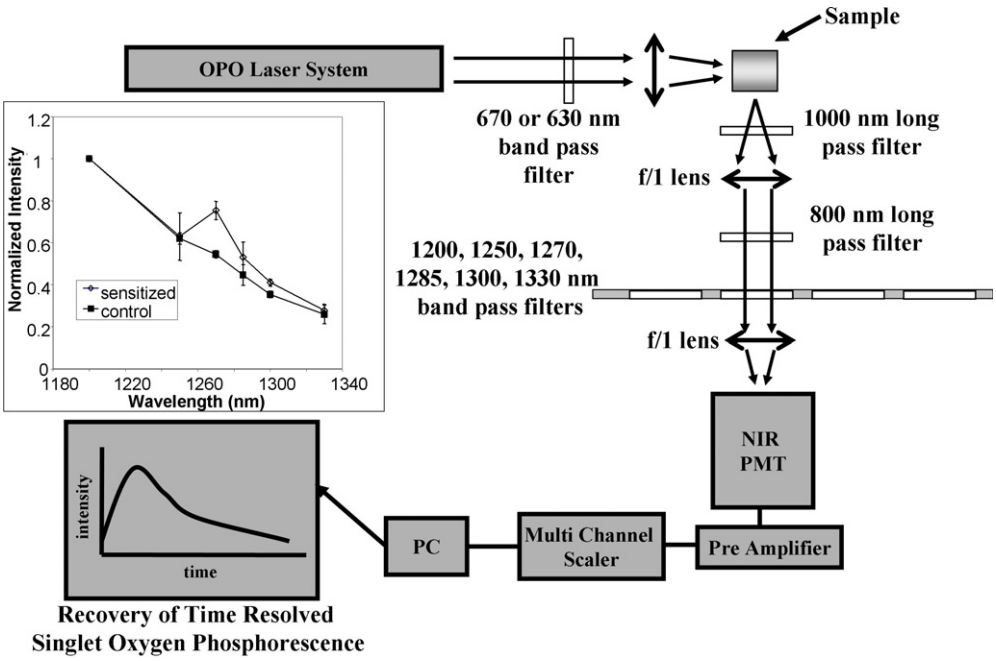


**Figure 17.** System used by Niedre *et al* (2002) for the direct detection of singlet oxygen *in vivo* during PDT. The luminescence spectra shown in the inset were measured on the skin of a rat injected with $AlPCS_4$ and on an uninjected control animal. While there is considerable background luminescence, the characteristic singlet oxygen peak at 1270 nm is evident.

in photochemistry of simple solutions. The challenge *in vivo* is that singlet oxygen reacts so rapidly that its ambient concentration during PDT is only in the picomolar range and the emission is several orders of magnitude weaker.

The first attempts in the late 1980s to measure infrared singlet oxygen luminescence in cells and tissues during PDT employed liquid nitrogen-cooled germanium detectors that had inadequate sensitivity for reliable measurements (Gorman and Rodgers 1992, Patterson *et al* 1990a, Rodgers 1988). About a decade later Hamamatsu Corp. introduced a photomultiplier tube (PMT) with high near-infrared quantum efficiency (∼1%). In the single-photon-counting mode and when cooled with liquid nitrogen, its noise equivalent power is about 100-fold lower than the germanium detector. This led to two groups reporting positive results for single oxygen detection *in vitro* and *in vivo*. The experimental setup used by Niedre *et al* (2002) is shown in figure 17. The PMT is fitted with a set of bandpass filters to provide coarse spectral resolution across the singlet oxygen emission peak at 1270 nm. Typical *in vivo* results in figure 17 show that there is considerable background signal at other wavelengths, probably due to phosphorescence of endogenous molecules in tissue and in optical components. There is also a strong fluorescence background that is eliminated by using pulsed laser excitation and time-resolved single-photon counting.

The initial papers by Niedre *et al* (2002) and Hirano *et al* (2002) demonstrated that the characteristic 1270 nm luminescence could be observed during PDT of animal tumors. Niedre *et al* (2003) went on to show that the cumulative singlet oxygen signal (i.e. the total number of photon counts during the PDT treatment) measured during PDT of tumor cell suspensions sensitized with ALA-PpIX correlated well with cell survival over a wide range of treatment

conditions. Subsequently, these authors performed a series of *in vivo* experiments in which the singlet oxygen luminescence was measured during ALA-PDT of normal mouse skin and the treatment irradiance was varied while keeping the total light exposure constant (Niedre *et al* 2005). In earlier work with this same animal model Robinson *et al* (1998) found that the skin response was greatest when the treatment was performed at the lowest irradiance and attributed this effect to photodynamically-induced oxygen depletion (see section 6.6). Niedre and co-workers found that the singlet oxygen signal was also reduced as the irradiance was increased and that there was a very good correlation between the cumulative $^1O_2$ signal and the independently measured skin response. As yet, there are no published reports of measurements during PDT of humans but this should be feasible during treatment of skin or other accessible lesions.

Although direct dosimetry of singlet oxygen appears possible and correlates with biological responses in pre-clinical models, there are number of potential limitations. First, the instrumentation is relatively complex and expensive. Second, it is not yet known how much the biological microenvironment may influence the relationship between the amount of singlet oxygen generated in the tissue and the actual emission at 1270 nm. Finally, the typical rate of 1270 nm light emission during PDT is only about $10^8$ photons cm$^{-3}$ s$^{-1}$. Assuming a detector quantum efficiency of 1%, light collection of 5% using $f/1$ optics, measurement time of 10 s, desired signal-to-noise ratio of 20:1 and $10^4$ dark counts per second, the minimum tissue volume required is $\sim$10 mm$^3$. This implies that it will not be possible to detect singlet oxygen with implanted optical fibers because the effective detection volume of such fibers is $<$1 mm$^3$ (see section 6.3) and the low numerical aperture of fibers in tissue further reduces the geometric collection efficiency. Recently, Yamamoto *et al* (2006) have successfully performed *in vivo* surface measurements using a 3.5 mm diameter fiber bundle. If luminescence measurements are restricted to an accessible surface, they can only be applied to a few disease sites. In addition, it may be challenging to interpret the data if the target volume is thick since the surface-biased singlet oxygen signal may not be representative of the PDT dose deeper in the target.

### *6.6. Dose-rate effects*

PDT dose-rate effects cause the biological response to depend not only on the local light fluence but also on the fluence rate and treatment time. These can be biological or physical in origin. As treatment times are extended and fluence rates lowered, cell repair and molecular responses to oxidative stress become important (Luna *et al* 1994, Oleinick and Evans 1998, Veenhuizen and Stewart 1995). It has also been shown that the dominant PDT cell-killing mechanism can shift from necrosis to apoptosis as the fluence rate is lowered, as in metronomic PDT (see section 8.1) (Bisland *et al* 2004). Here, we will focus on the photophysical mechanisms, namely photosensitizer ground-state depletion during pulsed irradiation and fluence-rate-dependent photochemical oxygen depletion.

It has long been known that PDT with short-pulse lasers can be less effective than with cw irradiation, even though the average fluence rate is the same (Sterenborg and vanGemert 1996). The reason for this is the finite number of photosensitizer molecules in the target volume. If a substantial fraction of these is raised to an excited state during the first part of a short laser pulse, photons in the rest of the pulse will be wasted because of a reduced probability of absorption and consequent singlet oxygen production. This effect can be estimated as follows.

PDT with cw light sources is usually performed at a maximum average fluence rate of about 100–200 mW cm$^{-2}$ to avoid thermal effects, so we will consider short-pulse irradiation at the same average fluence rate. We also assume that the pulse duration is short compared to

the photosensitizer excited-state lifetime so that the ground state is not repopulated during the pulse. If the local energy fluence per pulse is $H_0$ and the photosensitizer molecular absorption cross-section is $\sigma$ at the treatment wavelength $\lambda$, then, in order to have negligible ground-state depletion,

$$\frac{H_0 \sigma \lambda}{hc} \ll 1. \tag{11}$$

For a typical case where $\lambda = 630$ nm and $\sigma = 10^{-16}$ cm$^2$, $H_0$ should be much less than 3 mJ cm$^{-2}$. The pulse repetition frequency then must be much higher than 30 Hz to maintain the average fluence rate at 100 mW cm$^{-2}$. This is consistent with animal experiments that have shown reduced efficacy for PDT treatments performed with 10 Hz pulsed dye lasers. When lasers in the kHz range were used, the biological response was equivalent to that obtained with a cw light source (Panjehpour *et al* 1993).

The second physical mechanism for dose-rate effects is oxygen depletion. This occurs on a time scale of seconds and depends on the average fluence rate. The local rate of photochemical oxygen consumption, $\Gamma$, is equal to the rate of singlet oxygen generation, ignoring the minor contribution from singlet oxygen decay back to the ground state. For the energy fluence rate $E_0$, sensitizer concentration $[S_0]$ and singlet oxygen quantum yield $\phi$,

$$\Gamma = \frac{E_0 \lambda [S_0] \sigma \phi}{hc}. \tag{12}$$

For typical values ($H_0 = 100$ mW cm$^{-2}$, $[S_0] = 2$ $\mu$M, $\sigma = 10^{-16}$ cm$^2$, $\lambda = 630$ nm, $\phi = 0.5$), the consumption rate is 32 $\mu$M s$^{-1}$. This is considerably higher than the metabolic oxygen consumption rate of most tissues (Wang *et al* 2007), so it would not be surprising that the photochemical oxygen consumption can exceed the ability of the microvasculature to deliver oxygen to the irradiated tissue. Following Foster *et al* (1991), we can use diffusion theory to calculate the oxygen concentration as a function of distance from a single cylindrical capillary (diameter 10 $\mu$m) at various times after the initiation of PDT. For simplicity we assume that $[O_2]$ within the blood vessel is fixed at 80 $\mu$M, the metabolic oxygen consumption rate is 5 $\mu$M s$^{-1}$, the oxygen diffusion coefficient is $1.75 \times 10^{-5}$ cm$^2$ s$^{-1}$ and the PDT oxygen consumption rate is 32 $\mu$M s$^{-1}$. More complete models that incorporate oxygen gradients along the blood vessel have been described by Yuan *et al* (1997) and Wang *et al* (2007).) The results in figure 18(a) show that when irradiation begins, a new equilibrium is established within a few seconds in which $[O_2]$ is $<10$ $\mu$M over most of the tissue volume. Experiments with cell suspensions have shown that the efficacy of PDT is dramatically reduced at such levels, presumably because other pathways for sensitizer triplet de-excitation compete with energy transfer to ground-state oxygen (Moan and Sommer 1985, See *et al* 1984). When the fluence rate is reduced by an order of magnitude (figure 18(b), the oxygen concentration remains above 50 $\mu$M. Also shown in figure 18(c) is the calculated re-oxygenation of tissue when irradiation under the conditions of figure 18(a) is halted. These simple simulations suggest that PDT performed at low fluence rate or using an on–off illumination scheme can be more effective than PDT at continuous high fluence rate. We note that this oxygen effect can be much greater than the familiar decrease in the biological effectiveness of ionizing radiation under hypoxic conditions: in complete hypoxia, low-LET radiation is about three times less effective than under normoxia, but PDT is totally ineffective. However, it may still be possible to damage tissue by PDT-mediated vascular shutdown even when direct cell killing is oxygen limited. In addition, for some photosensitizers, oxygen-independent cytotoxic pathways may be important under $O_2$-limited conditions (Foote 1991) although this has not been exploited *in vivo* to date. The concept of two-photon/two-color PDT discussed in section 8.2 can also be used to circumvent the oxygen limitation of standard one-photon PDT.

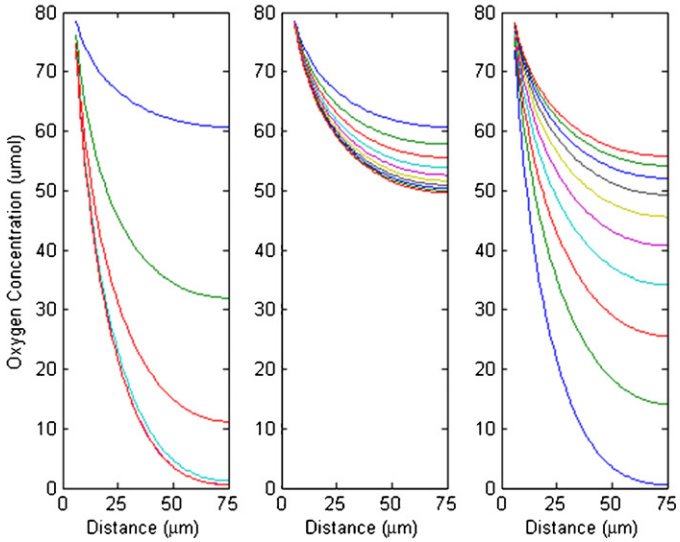


**Figure 18.** Calculations of oxygen concentration as a function of distance from the center of a single 10 $\mu$m diameter capillary. In the left graph, the top curve represents the initial equilibrium distribution before PDT. The remaining curves are calculated at 1 s intervals following the initiation of PDT under conditions that consume oxygen at the rate of 32 $\mu$M s$^{-1}$. A new equilibrium is rapidly established where PDT is ineffective throughout most of the tissue. The center graph shows the situation when the fluence rate is reduced by a factor of 10. Under these conditions, oxygenation is reduced but not enough to impair PDT. The right graph illustrates the recovery of oxygen from the depletion in the left graph when irradiation is terminated. Curves are plotted for 1 s intervals. The model assumes that oxygen concentration within the capillary is fixed at 80 $\mu$M and that the oxygen gradient is zero at 75 $\mu$m, half the inter-capillary distance.

The first systematic experimental studies of photochemical oxygen depletion and subsequent re-oxygenation were reported by Tromberg *et al* (1990), who performed non-invasive transcutaneous measurements of $pO_2$ using Clark-type oxygen electrodes placed over implanted tumors and normal skin on rabbit ear and showed that oxygen concentration was reversibly reduced during PDT irradiation. After a certain point, however, the oxygen depletion was permanent—probably as a result of treatment-induced vascular shutdown. Foster and co-workers (Foster *et al* 1991, Foster and Gao 1992) used a biophysical model similar to that described above (figure 18) to show that oxygen depletion was likely under typical PDT treatment conditions. Subsequent work by other groups using implanted oxygen electrodes has validated these modeling studies (Busch 2006, Chen *et al* 1996, 2002a, Henderson *et al* 2000). As mentioned in section 6.5, there is considerable biological evidence that PDT is less effective at high fluence rates (Busch 2006, Coutier *et al* 2002, Foster *et al* 1991, Henderson *et al* 2004, Robinson *et al* 1998) and in some cases this has been shown to result from photochemical depletion of tissue oxygen.

### *6.7. Dosimetry clinical case study: PDT of the prostate*

Here we illustrate some of the above points by considering a current clinical application of PDT, namely interstitial treatment of (locally-recurrent) prostate cancer. In this case the goal is to destroy tumor throughout the entire organ while sparing normal structures, including the rectum, bladder and urethra. Two groups have recently reported Phase II clinical studies: at the University of Pennsylvania (Du *et al* 2006) PDT has been performed 3 h after injection of

motexafin lutetium, a water-soluble, fluorescent sensitizer with an absorption peak at 732 nm; and at the University of Toronto (Weersink *et al* 2005) PDT at 762 nm is delivered 20 min after injection of the non-fluorescent agent, TOOKAD, a sensitizer that is rapidly cleared and so specifically targets the vasculature. Both groups employ a treatment technique borrowed from brachytherapy in which catheters, carrying diffusing optical fibers, are implanted in the prostate transperineally under transrectal ultrasound guidance.

The U. Penn. approach (Zhu *et al* 2005) is to implant 17G plastic catheters on a regular 1 cm grid. During treatment these catheters house cylindrical diffusing fibers with active lengths selected to match the size of the prostate at each grid location. An additional catheter is implanted centrally (0.5 cm from the closest treatment catheter) in each quadrant for dosimetry. Treatment light is delivered sequentially to the 4 quadrants. Before irradiation a single side-looking fiber is inserted into each dosimetry channel to map out the photosensitizer distribution by fluorescence, as described in section 6.3. Following this, isotropic fibers are inserted sequentially into each of the four dosimetry channels and an adjacent treatment channel. The isotropic source in the treatment catheter is activated at 732 nm and at low power (to avoid causing a PDT effect), and the isotropic detector is used to measure absolute fluence rate as the detector fiber is translated along the catheter using a stepping motor. These data (fluence rate *versus* position) are used to estimate the scattering and absorption coefficients by applying a diffusion model of light propagation and an iterative inverse method, as described in section 4.2. Similar measurements can be performed with a white light source and spectrally-resolved detection, so that absorption and scattering are calculated as functions of wavelength: the absorption spectrum can then be analyzed to estimate the local photosensitizer concentration, hemoglobin concentration (Hb and $HbO_2$) and oxygen saturation. Finally, the isotropic point source is removed and all of the cylindrical treatment fibers are inserted in the quadrant. During this treatment stage, the isotropic detector is used to measure the delivered fluence and the irradiation is adjusted so that a predetermined level (50–100 J $cm^{-2}$) is achieved. At present, this real-time light dosimetry is the only information used to control the PDT dose delivered, but there is potential for control based also on the photosensitizer and oxygen concentrations. Estimates of optical properties could also be used to map the PDT dose in 3D. This group has reported significant variations (up to a factor of 10) in the optical coefficients and the photosensitizer concentration within and between patients, which highlights the need to adjust the treatment accordingly.

The University of Toronto approach is closer to that currently used for brachytherapy, in that the treatment is pre-planned to deliver a minimum light fluence to the entire organ. Pre-treatment volumetric MRI scans are used for the plan and up to six diffusing fibers with different active lengths can be located within the prostate. A finite-element solution of the diffusion equation (equation (3)) is used to calculate the fluence rate in 3D. At present, it is assumed that the optical properties are uniform throughout the prostate and the values used in the planning are the averages for all prior patients. An additional constraint is that the treatment must be completed within about 30 min because of the rapid clearance of TOOKAD. Once an appropriate plan is devised, the treatment catheters are implanted using transrectal ultrasound and anatomical landmarks to duplicate the MR-based plan. Three additional catheters are inserted near the periphery and used to house isotropic detectors for measurement of the light fluence rate during the treatment. These measurements provide a direct check on the validity of the treatment plan and are also used to estimate the optical properties of the prostate: for this, the absorption and scattering coefficients are treated as free parameters in a diffusion model that relates the measured fluence rates to the known source powers. In contrast to the U. Penn. group, relatively low intra- or inter-patient variation has been found in the optical properties, possibly due to the longer wavelength (reduced effect of blood absorption). Plans

based on the updated averages give estimates of the fluence rate that are typically within 40% of those measured *in situ*. The estimated absorption coefficient can also be used to calculate the concentration of TOOKAD and the long-term goal is to incorporate this into the dose calculation in the planning. This group has also performed post-treatment MR scans in which PDT-induced necrosis can be identified. A reconstruction of the delivered treatment (including the actual source fiber positions determined on transrectal ultrasound and co-registered with the MR images) makes it possible to examine the correlation between necrosis and delivered light dose and facilitates, for example, generation of dose–response curves and dose–volume histograms analogous to those used in radiation treatment planning to assess the 'quality' of the dose distributions.

Finally, we note that researchers at the Lund Institute of Technology have developed a clinical system for interstitial PDT with on-line measurement of light fluence rate, sensitizer concentration and hemoglobin saturation. Its application during PDT of nodular basal call carcinomas has been reported (Thompson *et al* 2005) but it would also be a suitable tool for the prostate (Johansson *et al* 2007).

### *6.8. Treatment planning—is PDT dose important?*

We now return to the question raised at the beginning of this section—how accurately can and should the 'dose' be measured or calculated for PDT in clinical practice? The question might be rephrased as: what is the nature of the PDT dose response curve for normal and diseased tissues? Despite over two decades of activity, it is only recently that answers to this question have been forthcoming, since it has first been necessary to refine the concept of PDT dose as understanding of the biophysics and photobiology of PDT has developed, and to design, build and validate the models and instruments needed to measure the dose *in vivo*.

For example, in 2005 Zhou *et al* (2006) used the point fluorescence detection technique described in section 6.3 to demonstrate in an animal tumor model that knowledge of the photosensitizer uptake in individual tumors improved the predictability of treatment outcome and that the delivered light fluence could be adjusted to compensate for lower drug uptake. As described in the preceding section, the relationship between PDT dose and tissue necrosis can now also be examined for patients who received PDT for recurrent prostate cancer. Careful studies in animals and in the clinic over the next few years should provide the necessary information to guide treatment planning and delivery. Although it may be a daunting task to do this for all sensitizers and all disease sites, the capability to do this is now largely in place.

Unlike radiation therapy, many studies have shown that the PDT dose response usually has a threshold behavior, with a very sharp boundary between necrotic and grossly undamaged tissue on post-PDT histology. This has been associated with the concept that some minimum concentration of singlet oxygen is required to produce any particular biological effect in cells or tissues (Patterson *et al* 1990b). As pointed out by van Veen *et al* (2006), it is possible to achieve dramatic clinical responses with minimal effect on adjacent tissues, due to this threshold phenomenon. Nevertheless, other clinical studies have resulted in inadequate tumor responses or unacceptable complications. As these authors and others (Hahn *et al* 2006) have suggested, failure to realize the true potential of PDT is due, at least in part, to a failure to appreciate the complexity of PDT dosimetry and to use available state-of-the-art techniques to optimize PDT treatments for individual patients. A classic example of this was the demonstration, using *in situ* light dosimetry, in PDT of whole bladder wall for superficial recurrent cancer that the actual light fluence delivered could vary by a factor of up to 7-fold from patient to patient even for the same administered light energy (Star *et al* 1987), due to large variations in the wall reflectivity associated with vascularity. Failure to implement such

dosimetry led to unacceptable bladder wall damage leading to shrinkage. Hence, even though the tumor response rates were excellent and the treatment obtained governmental approvals, it never became accepted as a standard clinical method.

## 7. Tissue response monitoring

As discussed in section 3, the response of cells and tissues to PDT is complex and depends on the tissue and the specific PDT treatment parameters (Henderson and Dougherty 1992). From a practical perspective, it is useful to categorize the responses, and the techniques that can be used to monitor these *in vivo*, into delayed and prompt. Monitoring of delayed responses, occurring at some time (hours to days) following completion of treatment, is of value for determining outcome *versus* PDT dose relationships in clinical trials in order to determine the best average administered photosensitizer and light doses. In this case the monitoring serves as a surrogate for eventual clinical outcomes (e.g. disease-free survival). It can also be used to determine whether or not an adequate treatment was delivered, so that patients may be re-treated if necessary. Unlike most other therapies, the tissue responses in PDT, particularly vascular effects, may be very rapid. This offers the possibility to do dynamic, 'on line' monitoring of these prompt responses as a means to optimize treatment in individual patients.

A wide range of different monitoring techniques have been reported to date, although there are few extensive systematic studies for any of these, and there is a particular paucity of clinical reports. The methods include different forms of radiological imaging: x-ray computed tomography, magnetic resonance imaging (and spectroscopy), ultrasound and radionuclide imaging (both conventional gamma-ray imaging and positron emission tomography). White-light endoscopy has also been used commonly to evaluate completeness of PDT responses following treatment in, for example the GI tract, lung and bladder. CT (Betz *et al* 2007, Huang *et al* 2005), MRI (Gross *et al* 2003, Roth *et al* 2004) and ultrasound imaging (Ohlerth *et al* 2006, Yu *et al* 2005b) have demonstrated PDT-induced damage following treatment (delayed responses). In particular, it has been possible to see clearly the sharp boundary of damage in some tissues: figure 10(d) shows an example of gadolinium contrast-enhanced MRI of the prostate prior to and at 7 days following vascularly-targeted PDT (Haider *et al* 2007) where a large fraction of the total organ volume has been successfully treated. As discussed in section 6.7, such response images can be correlated with pre-treatment planning and *in situ* dosimetric information to refine treatment planning algorithms. Radionuclide imaging, including PET, has been used to track local functional and metabolic tissue responses (Berard *et al* 2006, Moore *et al* 1992).

In terms of measuring the prompt responses, most work to date has been focused on optical techniques, which are cost-effective and practical during PDT delivery, and primarily those that are sensitive to vascular changes. Some of these techniques have been applied in initial clinical tests. These include laser Doppler to detect altered blood flow (Wang *et al* 1997), diffuse reflectance and correlation spectroscopy to detect changes in both regional blood volume and/or hemoglobin oxygen saturation ($SO_2$) (Yu *et al* 2005b), and Doppler optical coherence tomography (DOCT) to measure altered blood flow at the level of individual microvessels (Aalders *et al* 2006, Chen *et al* 1998). Fluorescence angiography with injected dyes has also been used, both in tumors and in the eye to assess vascular responses directly (Woodhams *et al* 2004). The potential power of such prompt monitoring is seen in, for example, the work of Yodh and colleagues (Yu *et al* 2005b), who showed in a pre-clinical tumor xenograft model that changes in diffuse optical spectroscopy occurring during treatment correlated strongly with tumor growth delay (figure 19(a)). This promises the possibility that

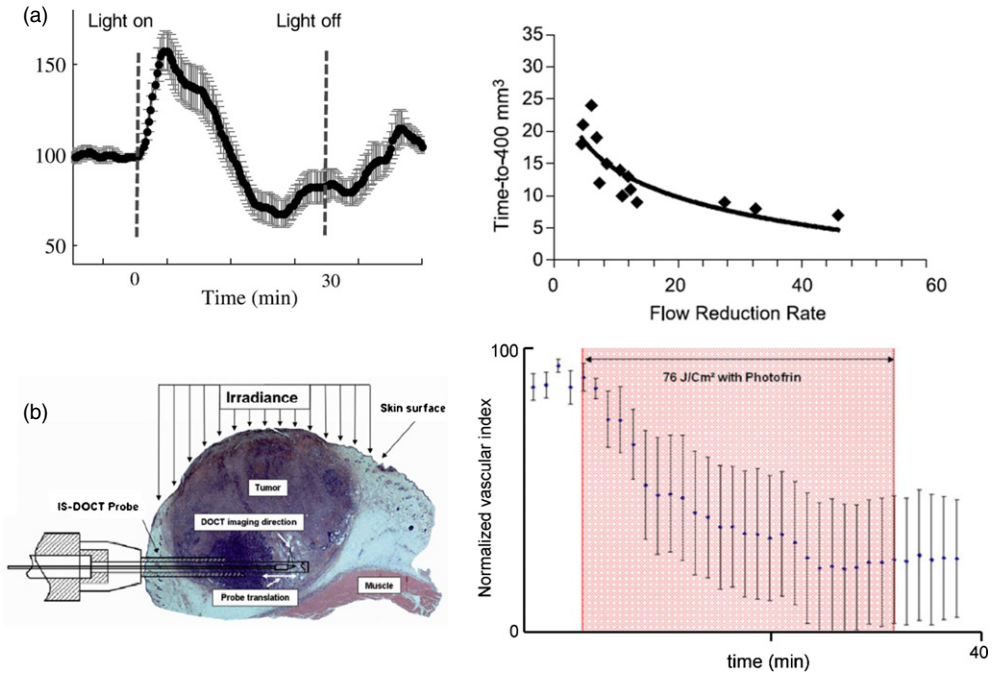


**Figure 19.** Examples of monitoring of PDT tumor responses. (a) Diffuse correlation spectroscopy (DCS) used to measure changes in blood flow in RIF tumors during Photofrin-PDT showing (left) the rapid vascular response during light irradiation and (right) the correlation between the time for tumor growth to a specified volume and the rate of blood flow decrease seen in the DCS curves (*adapted from* Yu *et al* (2005b)*, with permission from the American Association for Cancer Research*), (b) DOCT monitoring of PDT responses in a Dunning prostate tumor model using an interstitial fiber-optic probe (left), showing (right) a measure of the local microvasculature with blood flow above a threshold value as a function of time immediately before, during and after Photofrin-PDT treatment, averaged over several animals (*courtesy B Standish and colleagues*).

such methods could be applied on-line to modify the treatment and so minimize under- or over-dosing. The same methods have been demonstrated by this group in human prostate tumor PDT using the photosensitizer Texafrin (Yu *et al* 2006). These techniques yield volume-averaged vascular measures. Analogous studies are in progress using DOCT, both endoscopic (Standish *et al* 2007b) and interstitial (Standish *et al* 2007a) techniques (which have been demonstrated clinically), where the potential is to make highly localized measurements of the microvascular responses, as illustrated in figure 19(b). It remains to be seen whether volume-averaged or localized monitoring is more useful for different clinical applications.

For pre-clinical investigations, it is also possible to use techniques such as optical micro-imaging of gene expression using fluorescent proteins (Mitra *et al* 2003), bioluminescence imaging of both PDT-induced cell death and stress gene up-regulation (Moriyama *et al* 2004), high-frequency ultrasound imaging/power spectra of apoptosis through increased backscatter from condensed chromatin formation (Czarnota *et al* 1999), and electrical impedance spectroscopy of cell necrosis and apoptosis (Gersing *et al* 2003, Molckovsky and Wilson 2001).

## 8. Emerging developments in PDT

In this section, we will briefly consider some of the fundamental new directions for how PDT is administered and on which there is current active research and development. These include

- the use of low dose-rate administration of both photosensitizer and light over an extended period (metronomic PDT),
- at the other extreme, the use of ultrashort laser pulses to active the photosensitizer through two-photon processes,
- PDT 'molecular beacons', in which the photosensitizer is unactivated (quenched) until it interacts with target-specific molecules in the tissue,
- PDT using nanoparticles, either as photosensitizer delivery vehicles, as photosensitizers per se or as 'energy transducers'.

### *8.1. Metronomic PDT*

Conventionally, PDT is given as a single treatment using the highest photosensitizer dose that avoids systemic toxicity and skin photosensitivity and the highest light fluence rate that avoids tissue heating and photochemical depletion of oxygen. There have been a few studies of 'fractionated' PDT, particularly for treating skin tumors using ALA-PpIX, and improved responses have been reported compared to single doses: for example, the efficacy of ALA-PDT can be increased by giving a 'priming' light dose (20% of the total) 2 h prior to applying the remaining dose (de Haas *et al* 2007).

Several years ago, it was noted in both pre-clinical and clinical studies of PDT for brain tumors that, although the volume-average uptake of photosensitizer in normal brain may be very low, the brain is very sensitive to PDT damage, probably because the photosensitizer is localized in the vascular endothelial cells in regions with intact blood–brain barrier. Hence, this becomes the limiting factor to increasing the aggressiveness of treatment. However, it was subsequently shown that, using ALA-PpIX, it is possible to apply the drug and light at low rates so as to avoid causing any tissue necrosis (in either normal brain or tumor tissue), while producing apoptotic death specifically in tumor cells (Lilge *et al* 2000). By analogy to chemotherapy at low drug delivery rates, this approach has been termed metronomic, mPDT. The technical challenges in implementing this are: (a) how to administer the photosensitizer continuously, consistent with maintaining PpIX levels in the tumor cells and (b) how to deliver the light to the tumor also over several days or weeks. For the latter, in the case of brain tumors the options include implanting LED sources into the brain such as the linear LED arrays developed for interstitial and endoscopic treatments (Chen *et al* 2002b), implanting optical fibers connected through the skull to an external (laser) source or, in the same way, implanting a balloon applicator (Hirschberg *et al* 1999). The last approach is analogous to a method reported for brachytherapy of brain tumors. For other tumors sites, particularly skin lesions, the use of organic-LED 'patches' is one option that has recently been developed for continuous PDT to treat chronic infected wounds (Samuel 2007).

There are many questions unanswered in *m*PDT, including: is this concept valid for other photosensitizers besides ALA-PpIX?; is it valid for other malignant or benign conditions besides brain tumors?; and under what circumstances can one deliver the treatment fast enough to overcome target cell repopulation while keeping below the necrosis threshold? Nevertheless, the ability to 'bias' the tissue response to a specific mechanism of cell death is compelling.

### *8.2. Two-photon PDT*

Figure 20 illustrates two different forms of two-photon PDT, simultaneous (resonant) and two-photon/two-color. In the first (figure 20(a)), exposure of the photosensitizer to a short pulse of near-infrared light at $\lambda_{NIR}$ results in the absorption of two photons by the photosensitizer ground

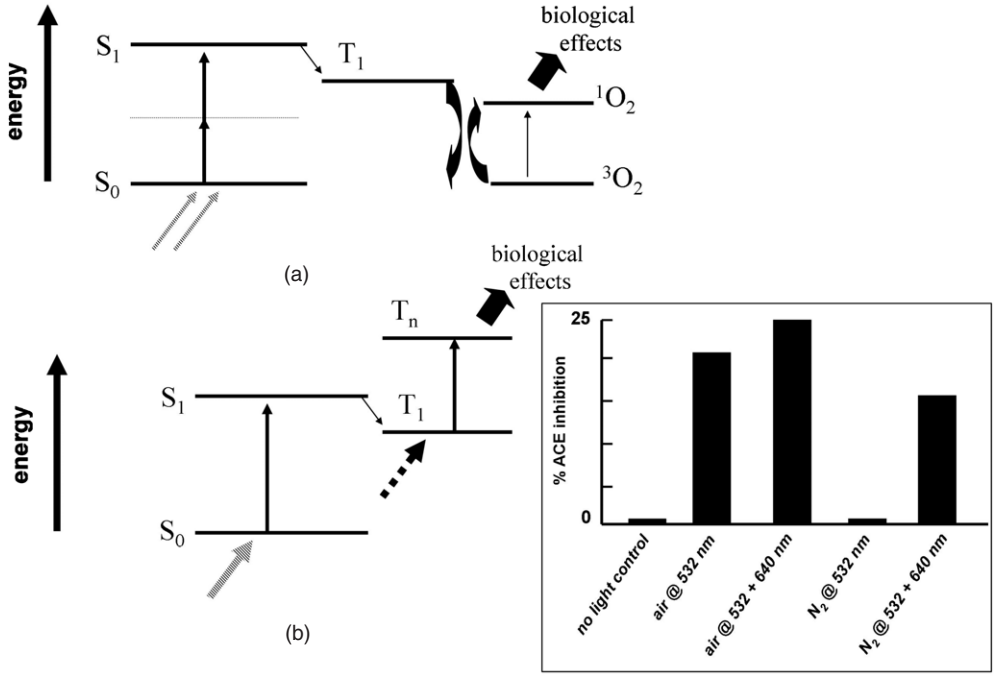


**Figure 20.** (a) Simultaneous absorption of two NIR photons raises the sensitizer to the $S_1$ excited state. (b) Sequential absorption of two photons, one from $S_0$ and the other from $T_1$, raises the sensitizer to a higher excited triplet state. The inset shows a measure of the PDT effect (inhibition of a specific enzyme, acetylcholinesterase) under fully aerated (air) and anoxic ($N_2$-purged) conditions, where there is no PDT effect for one-photon irradiation under $N_2$ but phototoxicity is still seen for two-photon/two-wavelength treatment (*adapted from* Smith *et al* (1994)*, with permission from Blackwell Synergy*).

state: in order for this to be effectively simultaneous, the light pulse must be typically shorter than ∼100 fs. The total energy absorbed is then same as that from one-photon absorption at $\lambda_{NIR}/2$ and the resulting photophysical and photochemical processes are the same (e.g. generation of singlet oxygen). In principle, this has two potential advantages.

The first advantage comes from the fact that the attenuation of NIR light is usually significantly lower than that of visible light (e.g. 800 versus 400 nm), due to reduced absorption (particularly of hemoglobin) and (to a lesser extent) scattering. Hence, in principle, it should be possible to treat more deeply in tissue (also assuming that the ratio of two-photon to one-photon absorption is higher for the photosensitizer than for other tissue components, which may require 'designer' drugs with this property). In practice, achieving greater depth of treatment may be limited. To understand this, consider the depth profile of singlet oxygen generation in tissue, taking for simplicity a single-exponential dependence for the light fluence rate versus depth, $z$. For one-photon activation at wavelength $\lambda_{NIR}/2$, the dependence is

$$[^1O_2](z) \propto [S_0]\sigma_1(\lambda_{NIR}/2)B(\lambda_{NIR}/2)E\exp(-z/\delta(\lambda_{NIR/2})) \tag{13}$$

where $[S_0]$ is the photosensitizer concentration, $\sigma_1$ is the one-photon cross-section of the photosensitizer, $B$ is the optical backscatter factor (typically ∼2–5, depending on the tissue absorption and scattering coefficients), $E$ is the incident irradiance on the tissue surface and $\delta$ is the effective penetration depth $(3\mu_a\mu_s')^{-1/2}$.

For two-photon excitation at $\lambda_{NIR}$, the dependence is given by

$$[^1O_2](z) \propto [S_0]\sigma_2(\lambda_{NIR})B(\lambda_{NIR})[E\ \exp(-z/\delta(\lambda_{NIR}))]^2$$
$$= [S_0]\sigma_2(\lambda_{NIR})B(\lambda_{NIR})E^2\ \exp(-2z/\delta(\lambda_{NIR})) \quad (14)$$

where $\sigma_2$ is the two-photon cross-section and the quadratic dependence comes from the fact that the probability of simultaneous absorption of two photons depends on the square of the local light fluence rate. Clearly then two-photon activation has a depth advantage if (a) the two-photon cross-section is high, which depends on the structure of the molecule, (b) if $E$ is high, which is the reason to use an ultrashort pulsed source that gives high instantaneous power without a large average power that would generate heat and (c) if the penetration depth of the light at the near-infrared wavelength is greater than twice the penetration depth at half this wavelength, i.e. if $\delta(\lambda_{NIR}) > 2\delta(\lambda_{NIR}/2)$. The first two factors are challenges to the synthetic chemist/photochemist and laser engineer, respectively. The last factor depends on the tissue type and on the particular wavelengths. As a general statement, highly melanotic or highly vascularized tissues are more likely to meet this condition as the penetration is a steeper function of increasing wavelength, see figure 2. Studies of 'deep' PDT treatment using two-photon PDT in cellular phantoms have been reported to achieve cell kill to a depth of 4 cm (Spangler *et al* 2006), but it is not clear if these adequately represent the absorption and scattering coefficients and spectra of tissues: initial *in vivo* studies in a subcutaneous mouse tumor model have achieved PDT damage at 1 cm depth without damage to overlying skin. A substantial challenge in such experiments is to ensure that the photoactivation is truly two-photon and not due to one-photon absorption of light that is multiply scattered in the tissue: since the two-photon absorption probability is very low, any residual long-wavelength tail on the one-photon absorption spectrum can contribute to the PDT effect.

The second potential advantage is that the quadratic dependence of the two-photon absorption probability can be exploited to give exquisite spatial confinement of the PDT effect by high numerical aperture focusing of a femtosecond activation laser beam. This effect is widely used in two-photon confocal microscopy to generate high resolution images (reflectance/transmission or fluorescence) in the focal plane, even through several hundred microns of tissue. Analogously, two-photon PDT is being investigated as a means to reduce the collateral damage to adjacent retinal structures in treatment of macular degeneration (AMD), as illustrated in figure 1. Two-photon closure of blood vessels has been demonstrated *in vivo* in a chick embryo model of neovascularization (Samkoe *et al* 2007) and the quadratic dependence of (endothelial) cell kill on the light intensity has recently been reported *in vitro* (Khurana *et al* 2007). The main technical questions in this approach are how fs beams will propagate in the eye and whether the limited numerical aperture and relatively poor optics of the eye, especially in the elderly, will compromise the spatial confinement. Technologically, the challenges include the development of affordable and reliable fs NIR laser sources, coupling of these into an ophthalmologic imaging/delivery instrument (e.g. confocal laser scanning ophthalmoscope) and designing/synthesizing two-photon photosensitizers with both very high two-photon cross-sections and good pharmacological properties.

The second class of two-photon activation (figure 20(b)) involves two separate short laser pulses, the first of which activates the photosensitizer to a singlet excited state. After a short time interval this transforms to the triplet state. A second laser pulse, at a wavelength that has high absorption in the triplet state, then generates higher excited triplet states that can interact directly with target biomolecules. The advantage of this is that the effects can be oxygen independent (Smith *et al* 1994). Thus, as illustrated in the inset to figure 20(b), the desired endpoint can be achieved even under hypoxic ($N_2$-saturated) conditions, which is particularly relevant to PDT of solid tumors. Again, however, the technical challenges to

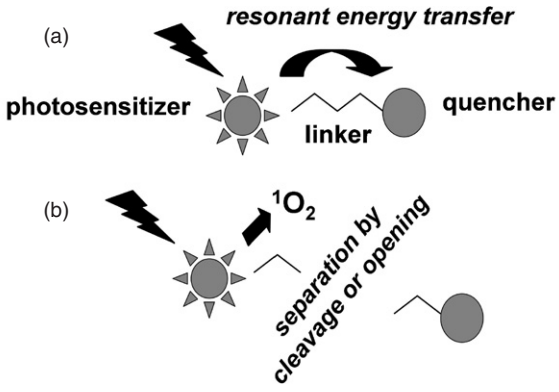


**Figure 21.** Concept of photodynamic molecular beacons. In (a), the generation of singlet oxygen is prevented by transfer of the excess energy in the photosensitizer upon light absorption to the nearby quencher. In (b), after spatial separation of the photosensitizer and quencher, singlet oxygen can be generated.

make this a clinical treatment are formidable. Firstly, photosensitizers are required that have high extinction coefficients in the ground and triplet states at reasonably long wavelengths, otherwise the depth of treatment will be very limited. Recently Houde and co-workers (Mir *et al* 2006) have reported phthalocyanine derivatives (with Cu as the metal ligand to manipulate the photophysical properties) that have ground-state and triplet-state absorptions at 670 and 514 nm, respectively. The latter is likely too short for general clinical utility. Secondly, double-pulsed laser sources are needed, preferably with some degree of wavelength tunability, and that are affordable and clinically practical. An interesting alternative is to use cw activation so that absorption takes place from both the photosensitizer ground and triplet states continuously and Mir *et al* (2008) showed this could cause photodynamic inactivation of an enzyme in a model system.

### *8.3. PDT molecular beacons*

The concept of PDT molecular beacons (PMB), introduced by G Zheng and colleagues (Juan *et al* 2004), is illustrated in figure 21. Analogous to the use of beacons for target-specific *in vivo* fluorescence imaging (Weissleder *et al* 1999), PMBs comprise a photosensitizer and a quencher, linked by a target-labile linker that keeps the photosensitizer and quencher in close proximity so that Fôrster resonant energy transfer (FRET) prevents activation of the photosensitizer. Upon interacting with the target, the linker is either broken or opened, so that the photosensitizer and quencher are separated, allowing the PDT action to occur. This has been demonstrated in solution, in cells and recently *in vivo* in an animal tumor model, using enzyme-cleavable peptide linkers (Zheng *et al* 2007). Work with anti-sense oligonucleotide 'loops' that are opened upon hybridization to target-cell-specific mRNA is in progress (Stefflova *et al* 2007). From the perspective of the physics and biophysics involved, PMBs are similar to conventional photosensitizers that are 'ON' all the time, but may be able to achieve a high level of target specificity that would markedly simplify light delivery and dosimetry since there would be minimal risk of damaging non-target tissues. Exploiting PMBs requires identification of a 'biomarker' that is overexpressed in the target tissue and against which the beacon can be designed. This fits well with current trends in molecular biology and molecular medicine.

### *8.4. Nanoparticle-based PDT*

As in many other areas of medical diagnostics and therapeutics (Ferrari 2005), recent advances in nanoparticle technology provide several different novel approaches to PDT (Wilson 2006), although this work is still at the proof-of-principle stage. Firstly, NPs can improve the delivery of photosensitizers, as they can with many other imaging contrast agents or therapeutic compounds. Examples are the incorporation of photosensitizers into modified silica NPs with antibody targeting, 'decorating' gold NPs with photosensitizers and the incorporation of photosensitizers into lipoprotein NPs. The advantages are that the loading (PS molecules per NP) can be very high and that the NPs can be decorated with a specific targeting moiety (e.g. antibody, peptide sequence, etc) so that the biodistribution no longer depends solely on the properties of the photosensitizer molecule itself.

Secondly, some NPs are themselves photoactive. Thus, for example, porous silicon NPs, that have a huge surface-to-volume ratio, are able to generate singlet oxygen upon light absorption through direct energy transfer (Kovalev and Fujii 2005). This has been demonstrated in solution using the $^1O_2$ luminescence technique discussed above. An interesting question is whether or not this $^1O_2$ generated within the porous matrix will be accessible to sensitive biotargets in cells, which will depend on both the microlocalization of the NPs and the $^1O_2$ lifetime. Another possibility is the use of carbon-60 (Bucky balls) as PDT agents that could be delivered as NPs with appropriate targeting agents (Yu *et al* 2005a). Their limitation is the relatively short wavelength absorption that peaks in the UV and falls off rapidly in the visible range: however, there may be applications where this is not limiting, as in topical anti-infective treatments.

The third novel class of PDT nanoparticle is the use of NP–PS conjugates, where the NP serves as the primary light absorber and then, through FRET, activates the photosensitizer. This principle has been demonstrated (Samia *et al* 2006) and the potential advantage is that the NP can be selected to have a very high photon cross-section at an optimal wavelength for the specific application, while the photosensitizer can be selected based, for example, on its high $^1O_2$ yield.

An issue with all these NP strategies is the delivery of the NPs or NP–PS conjugates to the target cells and tissues. One problem is that the pharmacokinetics are strongly dependent on the NP properties. For example, larger NPs can be trapped in the reticuloendothelial system (Fischer *et al* 2006). Potential toxicity can also be a concern (Samia *et al* 2006), especially if the NPs incorporate 'exotic' materials. Nevertheless, it is clear that the potential of NP-based PDT is such that there will be considerable research effort in this area.

## 9. Summary

While the original observation of photodynamic cell kill is over a century old, and the first patient treatment in the modern era took place in 1968, this concept is still evolving rapidly. The initial focus on treatment of patients with solid tumors has proven to be very challenging and, although PDT with various photosensitizers has been approved for a variety of cancer applications in many countries, it has not yet entered mainstream oncologic practice. This is perhaps surprising, considering it is complementary to established modalities. The medical physics community can make significant contributions in improving the accuracy and reliability of the treatment, in developing specialized technologies for light generation and delivery and for multi-factorial dosimetries and in applying state-of-the-art imaging techniques for monitoring tumor response (potentially on-line in real time). In age-related macular degeneration, PDT rapidly became the treatment of choice in the 1990s and over two million

patients have been treated worldwide. With the recent advent of anti-VEGF drugs for AMD, PDT is likely to evolve into a component of a multi-modal approach. The potential of PDT for controlling localized infection is rapidly emerging, driven by the major problem of antibiotic resistance. Both of these applications offer opportunities for biophysical sciences, as we have discussed.

As should be evident in particular from section 8, fundamental advances in PDT are far from exhausted. These new approaches are driven by new optical technologies (including spin-off from optical telecommunications), by advances in photosensitizer design and synthesis and molecularly-targeted drug delivery, by enabling tools and concepts from molecular biology and by the identification of new potential applications. The basic concept of drugs that are activated by light leads to the creation of a powerful 'platform' of technologies, so that we can expect PDT to continue to penetrate across a wide front of clinical applications and, although not discussed here, find many uses in post-genomic biology: an example of the latter is the recent work in tissue engineering using PDT to release growth factors along defined 'channels' in a 3D matrix to direct the growth of neurons (Luo and Shoichet 2004).

## Acknowledgments

The authors are grateful to the following for their current support of photodynamic therapy research: Canadian Cancer Society/National Cancer Institute of Canada, National Institutes of Health USA (PO1-CA43892), Canadian Institutes of Health Research, Canadian Institute for Photonic Innovations and the Ontario Institute for Cancer Research. We also thank our colleague, Tom Farrell, for performing the calculations in figures 6 and 18.

## References

Aalders M C G, Triesscheijn M, Ruevekamp M, de Bruin M, Baas P, Faber D J and Stewart F A 2006 Doppler optical coherence tomography to monitor the effect of photodynamic therapy on tissue morphology and perfusion *J. Biomed. Opt.* **11** 044011

Alexandrakis G, Farrell T J and Patterson M S 1998 Accuracy of the diffusion approximation in determining the optical properties of a two-layer turbid medium *Appl. Opt.* **37** 7401–9

Arridge S R, Hebden J C, Schwinger M, Schmidt F E W, Fry M E, Hillman E M C, Dehghani H and Delpy D T 2000 A method for three-dimensional time-resolved optical tomography *Int. J. Imaging Syst. Tech.* **11** 2–11

Arridge S R, Schweiger M, Hiraoka M and Delpy D T 1993 A finite-element approach for modeling photon transport in tissue *Med. Phys.* **20** 299–309

Barr H, Tralau C J, Boulos P B, MacRobert A J, Tilly R and Bown S G 1987 The contrasting mechanisms of colonic collagen damage between photodynamic therapy and thermal injury *Photochem. Photobiol.* **46** 795–800

Beek J F, Blokland P, Posthumus P, Aalders M, Pickering J W, Sterenborg H J C M and vanGemert M J C 1997 *In vitro* double-integrating-sphere optical properties of tissues between 630 and 1064 nm *Phys. Med. Biol.* **42** 2255–61

Ben Hur E 1998 Inactivation of pathogens in blood and blood products *Med. Health R. I.* **81** 396–9

Berard V, Lecomte R and Van Lier J E 2006 Positron emission tomography imaging of tumor response after photodynamic therapy *J. Environ. Pathol. Toxicol. Oncol.* **25** 239–49

Betz C S, Jager H R, Brookes J A, Richards R, Leunig A and Hopper C 2007 Interstitial photodynamic therapy for a symptom-targeted treatment of complex vascular malformations in the head and neck region *Lasers Surg. Med.* **39** 571–82

Biel M 2006 Advances in photodynamic therapy for the treatment of head and neck cancers *Lasers Surg. Med.* **38** 349–55

Bisland S K, Lilge L, Lin A, Rusnov R and Wilson B C 2004 Metronomic photodynamic therapy as a new paradigm for photodynamic therapy: rationale and preclinical evaluation of technical feasibility for treating malignant brain tumors *Photochem. Photobiol.* **80** 22–30

Boere I A, Robinson D J, de Bruijn H S, Kluin J, Tilanus H W, Sterenborg H J C M and de Bruin R W F 2006 Protoporphyrin IX fluorescence photobleaching and the response of rat Barrett's esophagus following 5-aminolevulinic acid photodynamic therapy *Photochem. Photobiol.* **82** 1638–44

Brancaleon L and Moseley H 2002 Laser and non-laser light sources for photodynamic therapy *Lasers Med. Sci.* **17** 173–86

Bressler N M *et al* 2005 Verteporfin therapy for subfoveal choroidal neovascularization in age-related macular degeneration: four-year results of an open-label extension of 2 randomized clinical trials: TAP Report No. 7 *Arch. Ophthalmol.* **123** 1283–5

Brown S B, Brown E A and Walker I 2004 The present and future role of photodynamic therapy in cancer treatment *Lancet Oncol.* **5** 497–508

Buerk D G 2004 Measuring tissue PO2 with microelectrodes *Methods Enzymol.* **381** 665–90

Burch S, Bogaards A, Siewerdsen J, Moseley D, Yee A, Finkelstein J, Weersink R, Wilson B C and Bisland S K 2005 Photodynamic therapy for the treatment of metastatic lesions in bone: studies in rat and porcine models *J. Biomed. Opt.* **10** 034011

Busch T M 2006 Local physiological changes during photodynamic therapy *Lasers Surg. Med.* **38** 494–9

Cengel K A, Glatstein E and Hahn S M 2007 Intraperitoneal photodynamic therapy *Cancer Treat. Res.* **134** 493–514

Chabrier-Rosello Y, Foster T H, Perez-Nazario N, Mitra S and Haidaris C G 2005 Sensitivity of *Candida albicans* germ tubes and biofilms to Photofrin-mediated phototoxicity *Antimicrob. Agents Chemother.* **49** 4288–95

Chen Q, Chen H and Hetzel F W 1996 Tumor oxygenation changes post-photodynamic therapy *Photochem. Photobiol.* **63** 128–31

Chen Q, Huang Z, Chen H, Shapiro H, Beckers J and Hetzel F W 2002a Improvement of tumor response by manipulation of tumor oxygenation during photodynamic therapy *Photochem. Photobiol.* **76** 197–203

Chen J, Keltner L, Christophersen J, Zheng F, Krouse M, Singhal A and Wang S S 2002b New technology for deep light distribution in tissue for phototherapy *Cancer J.* **8** 154–63

Chen Z P, Milner T E, Wang X J, Srinivas S and Nelson J S 1998 Optical Doppler tomography: imaging *in vivo* blood flow dynamics following pharmacological intervention and photodynamic therapy *Photochem. Photobiol.* **67** 56–60

Cheong W F, Prahl S A and Welch A J 1990 A review of the optical properties of biological tissues *IEEE J. Quantum Elect.* **26** 2166–85

Chou T M, Woodburn K W, Cheong W F, Lacy S A, Sudhir K, Adelman D C and Wahr D 2002 Photodynamic therapy: applications in atherosclerotic vascular disease with motexafin lutetium *Catheter. Cardiovasc. Interv.* **57** 387–94

Conover D L, Fenton B M, Foster T H and Hull E L 2000 An evaluation of near infrared spectroscopy and cryospectrophotometry estimates of haemoglobin oxygen saturation in a rodent mammary tumour model *Phys. Med. Biol.* **45** 2685–700

Coutier S, Bezdetnaya L N, Foster T H, Parache R M and Guillemin F 2002 Effect of irradiation fluence rate on the efficacy of photodynamic therapy and tumor oxygenation in *meta*-tetra(hydroxyphenyl)chlorin (mTHPC)-sensitized HT29 xenografts in nude mice *Radiat. Res.* **158** 339–45

Czarnota G J, Kolios M C, Abraham J, Portnoy M, Ottensmeyer F P, Hunt J W and Sherar M D 1999 Ultrasound imaging of apoptosis: high-resolution non-invasive monitoring of programmed cell death *in vitro*, *in situ* and *in vivo Br. J. Cancer* **81** 520–7

Davies N 2006 Development of metronomic photodynamic therapy as a treatment for newly initiated brain tumors *MSc Thesis* University of Toronto

de Haas E R M, de Vijlder H C, Sterenborg H J C M, Neumann H A M and Robinson D J 2007 Fractionated aminolevulinic acid-photodynamic therapy provides additional evidence for the use of PDT for non-melanoma skin cancer *J. Eur. Acad. Dermatol. Venereol.* doi:10.1111/j.1468–3083.200702445x

Delpy D T, Cope M, Vanderzee P, Arridge S, Wray S and Wyatt J 1988 Estimation of optical pathlength through tissue from direct time of flight measurement *Phys. Med. Biol.* **33** 1433–42

Demidova T N and Hamblin M R 2004 Photodynamic therapy targeted to pathogens *Int. J. Immunopathol. Pharmacol.* **17** 245–54

Diamond K R, Farrell T J and Patterson M S 2003a Measurement of fluorophore concentrations and fluorescence quantum yield in tissue-simulating phantoms using three diffusion models of steady-state spatially resolved fluorescence *Phys. Med. Biol.* **48** 4135–49

Diamond K R, Patterson M S and Farrell T J 2003b Quantification of fluorophore concentration in tissue-simulating media by fluorescence measurements with a single optical fiber *Appl. Opt.* **42** 2436–42

Dougherty T J, Kaufman J E, Goldfarb A, Weishaupt K R, Boyle D and Mittleman A 1978 Photoradiation therapy for treatment of malignant tumors *Cancer Res.* **38** 2628–35

Dougherty T J, Lawrence G, Kaufman J H, Boyle D, Weishaupt K R and Goldfarb A 1979 Photoradiation in the treatment of recurrent breast carcinoma *J. Natl Cancer Inst.* **62** 231–7

Du K L *et al* 2006 Preliminary results of interstitial motexafin lutetium-mediated PDT for prostate cancer *Lasers Surg. Med.* **38** 427–34

Dysart J S and Patterson M S 2005 Characterization of Photofrin photobleaching for singlet oxygen dose estimation during photodynamic therapy of MLL cells *in vitro Phys. Med. Biol.* **50** 2597–616

Dysart J S and Patterson M S 2006 Photobleaching kinetics, photoproduct formation, and dose estimation during ALA induced PpIX PDT of MLL cells under well oxygenated and hypoxic conditions *Photochem. Photobiol. Sci.* **5** 73–81

Dysart J S, Singh G and Patterson M S 2005 Calculation of singlet oxygen dose from photosensitizer fluorescence and photobleaching during mTHPC photodynamic therapy of MLL cells *Photochem. Photobiol.* **81** 196–205

Eggener S E *et al* 2007 Focal therapy for localized prostate cancer: a critical appraisal of rationale and modalities *J. Urol.* **178** 2260–7

Farrell T J, Patterson M S, Hayward J E, Wilson B C and Beck E R 1994 A CCD and neural network based instrument for the non-invasive determination of tissue optical properties *in-vivo SPIE Proc.* **2135** 117–28

Farrell T J, Wilson B C, Patterson M S and Olivo M C 1998 Comparison of the *in vivo* photodynamic threshold dose for Photofrin, mono- and tetrasulfonated aluminum phthalocyanine using a rat liver model *Photochem. Photobiol.* **68** 394–9

Ferrari M 2005 Cancer nanotechnology: opportunities and challenges *Nat. Rev. Cancer* **5** 161–71

Fien S M and Oseroff A R 2007 Photodynamic therapy for non-melanoma skin cancer *J. Natl Compr. Canc. Netw.* **5** 531–40

Finlay J C and Foster T H 2004 Hemoglobin oxygen saturations in phantoms and *in vivo* from measurements of steady-state diffuse reflectance at a single, short source–detector separation *Med. Phys.* **31** 1949–59

Finlay J C, Mitra S, Patterson M S and Foster T H 2004 Photobleaching kinetics of Photofrin *in vivo* and in multicell tumour spheroids indicate two simultaneous bleaching mechanisms *Phys. Med. Biol.* **49** 4837–60

Firbank M, Hiraoka M, Essenpreis M and Delpy D T 1993 Measurement of the optical properties of the skull in the wavelength range 650–950 nm *Phys. Med. Biol.* **38** 503–10

Fischer H C, Liu L C, Pang K S and Chan W C W 2006 Pharmacokinetics of nanoscale quantum dots: *in vivo* distribution, sequestration, and clearance in the rat *Adv. Funct. Mater.* **16** 1299–305

Flock S T, Wilson B C and Patterson M S 1987 Total attenuation coefficients and scattering phase functions of tissues and phantom materials at 633 nm *Med. Phys.* **14** 835–41

Foote C S 1991 Definition of Type-I and Type-II photosensitized oxidation *Photochem. Photobiol.* **54** 659

Forrer M, Glanzmann T, Braichotte D, Wagnieres G, van den Bergh H, Savary J F and Monnier P 1995 *In vivo* measurement of fluorescence bleaching of meso-tetrahydroxyphenyl chlorin (mTHPC) in the esophagus and oral cavity *SPIE Proc.* **2627** 33–9

Foster T H and Gao L 1992 Dosimetry in photodynamic therapy—oxygen and the critical importance of capillary density *Radiat. Res.* **130** 379–83

Foster T H, Murant R S, Bryant R G, Knox R S, Gibson S L and Hilf R 1991 Oxygen consumption and diffusion effects in photodynamic therapy *Radiat. Res.* **126** 296–303

Funke B, Jungel A, Schastak S, Wiedemeyer K, Emmrich F and Sack U 2006 Transdermal photodynamic therapy—a treatment option for rheumatic destruction of small joints? *Lasers Surg. Med.* **38** 866–74

Gersing E, Kelleher D K and Vaupel P 2003 Tumour tissue monitoring during photodynamic and hyperthermic treatment using bioimpedance spectroscopy *Physiol. Meas.* **24** 625–37

Ghosh N, Mohanty S K, Majumder S K and Gupta P K 2001 Measurement of optical transport properties of normal and malignant human breast tissue *Appl. Opt.* **40** 176–84

Gibson A P, Hebden J C and Arridge S R 2005 Recent advances in diffuse optical imaging *Phys. Med. Biol.* **50** R1–43

Gold M H 2007 Acne and PDT: new techniques with lasers and light sources *Lasers Med. Sci.* **22** 67–72

Gomer C J, Luna M, Ferrario A, Wong S, Fisher A M and Rucker N 1996 Cellular targets and molecular responses associated with photodynamic therapy *J. Clin. Laser Med. Surg.* **14** 315–21

Gorman A A and Rodgers M A J 1992 Current perspectives of singlet oxygen detection in biological environments *J. Photochem. Photobiol. B: Biol.* **14** 159–76

Gross S, Gilead A, Scherz A, Neeman M and Salomon Y 2003 Monitoring photodynamic therapy of solid tumors online by BOLD-contrast MRI *Nat. Med.* **9** 1327–31

Hahn S M, Putt M E, Metz J, Shin D B, Rickter E, Menon C, Smith D, Glatstein E, Fraker D L and Busch T M 2006 Photofrin uptake in the tumor and normal tissues of patients receiving intraperitoneal photodynamic therapy *Clin. Cancer Res.* **12** 5464–70

Haider M A *et al* 2007 Prostate gland: MR imaging appearance after vascular targeted photodynamic therapy with palladium-bacteriopheophorbide *Radiology* **244** 196–204

Henderson B W, Busch T M and Snyder J W 2006 Fluence rate as a modulator of PDT mechanisms *Lasers Surg. Med.* **38** 489–93

Henderson B W and Dougherty T J 1992 How does photodynamic therapy work *Photochem. Photobiol.* **55** 145–57

Henderson B W, Gollnick S O, Snyder J W, Busch T M, Kousis P C, Cheney R T and Morgan J 2004 Choice of oxygen-conserving treatment regimen determines the inflammatory response and outcome of photodynamic therapy of tumors *Cancer Res.* **64** 2120–6

Henderson B W *et al* 2000 Photofrin photodynamic therapy can significantly deplete or preserve oxygenation in human basal cell carcinomas during treatment, depending on fluence rate *Cancer Res.* **60** 525–9

Hetzel F W, Brahmavar S M, Chen Q, Jacques S L, Patterson M S, Wilson B C and Zhu T C 2005 *Photodynamic therapy dosimetry* (Madison, WI: Medical Physics Publishing) *AAPM Report 88*

Hirano T, Kohno E and Nishiwaki M 2002 Detection of near infrared emission from singlet oxygen in PDT with an experimental tumor bearing mouse *J. Japan. Soc. Laser Surg. Med.* **22** 99–108

Hirschberg H, Madsen S, Lote K, Pham T and Tromberg B 1999 An indwelling brachytherapy balloon catheter: potential use as an intracranial light applicator for photodynamic therapy *J. Neurooncol.* **44** 15–21

Hopper C, Kubler A, Lewis H, Tan I B and Putnam G 2004 mTHPC-mediated photodynamic therapy for early oral squamous cell carcinoma *Int. J. Cancer* **111** 138–46

Huang Z, Chen Q, Luck D, Beckers J, Wilson B C, Trncic N, Larue S M, Blanc D and Hetzel F W 2005 Studies of a vascular-acting photosensitizer, Pd-bacteriopheophorbide (TOOKAD), in normal canine prostate and spontaneous canine prostate cancer *Lasers Surg. Med.* **36** 390–7

Jacques S L 1998 Light distributions from point, line and plane sources for photochemical reactions and fluorescence in turbid biological tissues *Photochem. Photobiol.* **67** 23–32

Jarvi M T, Niedre M J, Patterson M S and Wilson B C 2006 Singlet oxygen luminescence dosimetry (SOLD) for photodynamic therapy: current status, challenges and future prospects *Photochem. Photobiol.* **82** 1198–210

Jeeves W P, Wilson B C, Firnau G and Brown K 1985 Studies of HPD and radiolabeled HPD *in vivo* and *in vitro Adv. Exp. Med. Biol.* **193** 51–67

Johansson A, Axelsson J and Andersson-Engels S 2007 Realtime light dosimetry software tools for interstitial photodynamic therapy of the human prostate *Med. Phys.* **34** 4309–21

Jori G and Brown S B 2004 Photosensitized inactivation of microorganisms *Photochem. Photobiol. Sci.* **3** 403–5

Juan C, Stefflova K, Niedre M J, Wilson B C, Chance B, Glickson J D and Gang Z 2004 Protease-triggered photosensitizing beacon based on singlet oxygen quenching and activation *J. Am. Chem. Soc.* **126** 11450–1

Key H, Davies E R, Jackson P C and Wells P N T 1991 Optical attenuation characteristics of breast tissues at visible and near-infrared wavelengths *Phys. Med. Biol.* **36** 579–90

Khurana M, Collins H A, Karotki A, Anderson H L, Cramb D T and Wilson B C 2007 Quantitative *in vitro* demonstration of two-photon photodynamic therapy using Photofrin ® and Visudyne® *Photochem. Photobiol.* **83** 1441–8

Kovalev D and Fujii M 2005 Silicon nanocrystals: photosensitizers for oxygen molecules *Adv. Mater.* **17** 2531–44

Lilge L, Portnoy M and Wilson B C 2000 Apoptosis induced *in vivo* by photodynamic therapy in normal brain and intracranial tumour tissue *Br. J. Cancer* **83** 1110–17

Luna M C, Wong S and Gomer C J 1994 Photodynamic therapy mediated induction of early response genes *Cancer Res.* **54** 1374–80

Luo Y and Shoichet M S 2004 A photolabile hydrogel for guided three-dimensional cell growth and migration *Nat. Mater.* **3** 249–53

Maisch T 2007 Anti-microbial photodynamic therapy: useful in the future? *Lasers Med. Sci.* **22** 83–91

Marijnissen J P A and Star W M 1996 Calibration of isotropic light dosimetry probes based on scattering bulbs in clear media *Phys. Med. Biol.* **41** 1191–208

Marijnissen J P A and Star W M 2002 Performance of isotropic light dosimetry probes based on scattering bulbs in turbid media *Phys. Med. Biol.* **47** 2049–58

Markel V A 2004 Modified spherical harmonics method for solving the radiative transport equation *Waves Random Media* **14** L13–9

Mazor O, Brandis A, Plaks V, Neumark E, Rosenbach-Belkin V, Salomon Y and Scherz A 2005 WST11: a novel water-soluble bacteriochlorophyll derivative; cellular uptake, pharmacokinetics, biodistribution and vascular-targeted photodynamic activity using melanoma tumors as a model *Photochem. Photobiol.* **81** 342–51

Mennel S, Barbazetto I, Meyer C H, Peter S and Stur M 2007 Ocular photodynamic therapy—standard applications and new indications (Part 1) *Ophthalmologica* **221** 216–26

Mir Y, Houde D and Van Lier J E 2006 Two-photon absorption of copper tetrasulfophthalocyanine induces phototoxicity towards Jurkat cells *in vitro Photochem. Photobiol. Sci.* **5** 1024–30

Mir Y, Houde D and Van Lier J E 2008 Photodynamic inhibition of acetylcholinesterase after two-photon excitation of copper tetrasulfophthalocyanine *Lasers Med. Sci.* **23** 19–25

Mitra S, Goren E M, Frelinger J G and Foster T H 2003 Activation of heat shock protein 70 promoter with meso-tetrahydroxyphenyl chlorin photodynamic therapy reported by green fluorescent protein *in vitro* and *in vivo Photochem. Photobiol.* **78** 615–22

Miyagi K, Sampson R W, Sieber-Blum M and Sieber F 2003 Crystal violet combined with merocyanine 540 for the *ex vivo* purging of hematopoietic stem cell grafts *J. Photochem. Photobiol.* **70** 133–44

Moan J and Peng Q 2003 An outline of the hundred-year history of PDT *Anticancer Res.* **23** 3591–600

Moan J and Sommer S 1985 Oxygen dependence of the photosensitizing effect of hematoporphyrin derivative in NHIK 3025 cells *Cancer Res.* **45** 1608–10

Molckovsky A and Wilson B C 2001 Monitoring of cell and tissue responses to photodynamic therapy by electrical impedance spectroscopy *Phys. Med. Biol.* **46** 983–1002

Moore R B, Chapman J D, Mokrzanowski A D, Arnfield M R, Mcphee M S and Mcewan A J 1992 Noninvasive monitoring of photodynamic therapy with Tc-99 HMPAO scintigraphy *Br. J. Cancer* **65** 491–7

Moriyama E H, Bisland S K, Lilge L and Wilson B C 2004 Bioluminescence imaging of the response of rat gliosarcoma to ALA-PpIX-mediated photodynamic therapy *Photochem. Photobiol.* **80** 242–9

Moseley H, Allen J W, Ibbotson S, Lesar A, McNeill A, Camacho-Lopez M A, Samuel I D, Sibbett W and Ferguson J 2006 Ambulatory photodynamic therapy: a new concept in delivering photodynamic therapy *Br. J. Dermatol.* **154** 747–50

Nestor M S *et al* 2006 The use of photodynamic therapy in dermatology: results of a consensus conference *J. Drugs Dermatol.* **5** 140–54

Niedre M, Patterson M S and Wilson B C 2002 Direct near-infrared luminescence detection of singlet oxygen generated by photodynamic therapy in cells *in vitro* and tissues *in vivo Photochem. Photobiol.* **75** 382–91

Niedre M J, Secord A J, Patterson M S and Wilson B C 2003 *In vitro* tests of the validity of singlet oxygen luminescence measurements as a dose metric in photodynamic therapy *Cancer Res.* **63** 7986–94

Niedre M J, Yu C S, Patterson M S and Wilson B C 2005 Singlet oxygen luminescence as an *in vivo* photodynamic therapy dose metric: validation in normal mouse skin with topical amino-levulinic acid *Br. J. Cancer* **92** 298–304

Nseyo U O, DeHaven J, Dougherty T J, Potter W R, Merrill D L, Lundahl S L and Lamm D L 1998 Photodynamic therapy (PDT) in the treatment of patients with resistant superficial bladder cancer: a long-term experience *J. Clin. Laser Med. Surg.* **16** 61–8

Nyst H J, van Veen R L P, Tan I B, Peters R, Spaniol S, Robinson D J, Stewart F A, Levendag P C and Sterenborg H J 2007 Performance of a dedicated light delivery and dosimetry device for photodynamic therapy of nasopharyngeal carcinoma: phantom and volunteer experiments *Lasers Surg. Med.* **39** 647–53

Ohlerth S, Laluhova D, Buchholz J, Roos M, Walt H and Kaser-Hotz B 2006 Changes in vascularity and blood volume as a result of photodynamic therapy can be assessed with power Doppler ultrasonography *Lasers Surg. Med.* **38** 229–34

Oleinick N L and Evans H H 1998 The photobiology of photodynamic therapy: cellular targets and mechanisms *Radiat. Res.* **150** S146–56

Overholt B F *et al* 2007 Five-year efficacy and safety of photodynamic therapy with Photofrin in Barrett's high-grade dysplasia *Gastrointest. Endosc.* **66** 460–8

Pandey S K *et al* 2005 Multimodality agents for tumor imaging (PET, fluorescence) and photodynamic therapy. A possible see and treat approach *J. Med. Chem.* **48** 6286–95

Panjehpour M, Overholt B F, Denovo R C, Petersen M G and Sneed R E 1993 Comparative study between pulsed and continuous-wave lasers for Photofrin® photodynamic therapy *Lasers Surg. Med.* **13** 296–304

Papkovsky D B 2004 Methods in optical oxygen sensing: Protocols and critical analyses *Methods Enzymol.* **381** 715–35

Patterson M S, Madsen S J and Wilson B C 1990a Experimental tests of the feasibility of singlet oxygen luminescence monitoring *in vivo* during photodynamic therapy *J. Photochem. Photobiol.* **5** 69–84

Patterson M S, Wilson B C and Graff R 1990b *In vivo* tests of the concept of photodynamic threshold dose in normal rat liver photosensitized by aluminum chlorosulphonated phthalocyanine *Photochem. Photobiol.* **51** 343–9

Patterson M S, Wilson B C and Wyman D R 1990c The propagation of optical radiation in tissue: I. Models of radiation transport and their application *Lasers Med. Sci.* **6** 155–68

Peters V G, Wyman D R, Patterson M S and Frank G L 1990 Optical properties of normal and diseased human breast tissues in the visible and near infrared *Phys. Med. Biol.* **35** 1317–34

Pickering J W, Prahl S A, Vanwieringen N, Beek J F, Sterenborg H J C M and vanGemert M J C 1993 Double-integrating-sphere system for measuring the optical properties of tissue *Appl. Opt.* **32** 399–410

Pogue B W and Burke G 1998 Fiber-optic bundle design for quantitative fluorescence measurement from tissue *Appl. Opt.* **37** 7429–36

Pogue B W, Geimer S, McBride T O, Jiang S D, Osterberg U L and Paulsen K D 2001 Three-dimensional simulation of near-infrared diffusion in tissue: boundary condition and geometry analysis for finite-element image reconstruction *Appl. Opt.* **40** 588–600

Popp A K, Valentine M T, Kaplan P D and Weitz D A 2003 Microscopic origin of light scattering in tissue *Appl. Opt.* **42** 2871–80

Redmond R W and Gamlin J N 1999 A compilation of singlet oxygen yields from biologically relevant molecules *Photochem. Photobiol.* **70** 391–475

Rendon A, Weersink R and Lilge L 2006 Towards conformal light delivery using tailored cylindrical diffusers: attainable light dose distributions *Phys. Med. Biol.* **51** 5967–75

Robinson D J, de Bruijn H S, van der Veen N, Stringer M R, Brown S B and Star W M 1998 Fluorescence photobleaching of ALA-induced protoporphyrin IX during photodynamic therapy of normal hairless mouse skin: the effect of light dose and irradiance and the resulting biological effect *Photochem. Photobiol.* **67** 140–9

Rodgers M A J 1988 On the problems involved in detecting luminescence from singlet oxygen in biological specimens *J. Photochem. Photobiol. B: Biol.* **1** 371–3

Rogers D W O 2006 Fifty years of Monte Carlo simulations for medical physics *Phys. Med. Biol.* **51** R287–301

Roth Y, Tichler T, Kostenich G, Ruiz-Cabello J, Maier S E, Cohen J S, Orenstein A and Mardor Y 2004 High-*b*-value diffusion-weighted MR imaging for pretreatment prediction and early monitoring of tumor response to therapy in mice *Radiology* **232** 685–92

Samia A C, Dayal S and Burda C 2006 Quantum dot-based energy transfer: perspectives and potential for applications in photodynamic therapy *Photochem. Photobiol.* **82** 617–25

Samkoe K S, Clancy A A, Karotki A, Wilson B C and Cramb D T 2007 Complete blood vessel occlusion in the chick chorioallantoic membrane using two-photon excitation photodynamic therapy: implications for treatment of wet age-related macular degeneration *J. Biomed. Opt.* **12** 034025

Samuel I 2007 Light fantastic *Materials World* 28–30 August

Schmitt J M and Kumar G 1998 Optical scattering properties of soft tissue: a discrete particle model *Appl. Opt.* **37** 2788–97

See K L, Forbes I J and Betts W H 1984 Oxygen dependency of photocytotoxicity with hematoporphyrin derivative *Photochem. Photobiol.* **39** 631–4

Sheng C, Pogue B W, Wang E, Hutchins J E and Hoopes P J 2004 Assessment of photosensitizer dosimetry and tissue damage assay for photodynamic therapy in advanced-stage tumors *Photochem. Photobiol.* **79** 520–5

Sheppard C J R 2007 Fractal model of light scattering in biological tissue and cells *Opt. Lett.* **32** 142–4

Simpson C R, Kohl M, Essenpreis M and Cope M 1998 Near-infrared optical properties of *ex vivo* human skin and subcutaneous tissues measured using the Monte Carlo inversion technique *Phys. Med. Biol.* **43** 2465–78

Smith G, McGimpsey W G, Lynch M C, Kochevar I E and Redmond R W 1994 An efficient oxygen independent 2-photon photosensitization mechanism *Photochem. Photobiol.* **59** 135–9

Smits T, Kleinpenning M M, van Erp P E, van de Kerkhof P C and Gerritsen M J 2006 A placebo-controlled randomized study on the clinical effectiveness, immunohistochemical changes and protoporphyrin IX accumulation in fractionated 5-aminolevulinic acid—photodynamic theraphy in patients with psoriasis *Br. J. Dermatol.* **155** 429–36

Spangler J W, Starkey J R, Rebane A, Meng F, Gong A and Drobizhev I 2006 Synthesis, characterization, and preclinical studies of two-photon-activated targeted PDT therapeutic triads *SPIE Proc.* **6139** 61390X

Standish B A, Jin X, Smolen J, Mariampillai A, Munce N R, Wilson B C, Vitkin I A and Yang V X 2007a Interstitial Doppler optical coherence tomography monitors microvascular changes during photodynamic therapy in a Dunning prostate model under varying treatment conditions *J. Biomed. Opt.* **12** 034022

Standish B A, Yang V X, Munce N R, Wong Kee, Song L M, Gardiner G, Lin A, Mao Y I, Vitkin A, Marcon N E and Wilson B C 2007b Doppler optical coherence tomography monitoring of microvascular tissue response during photodynamic therapy in an animal model of Barrett's esophagus *Gastrointest. Endosc.* **66** 326–33

Star W M, Marijnissen H P A, Jansen H, Keijzer M and vanGemert M J C 1987 Light dosimetry for photodynamic therapy by whole bladder wall irradiation *Photochem. Photobiol.* **46** 619–24

Stefflova K, Chen J and Zheng G 2007 Killer beacons for combined cancer imaging and therapy *Curr. Med. Chem.* **14** 2110–25

Sterenborg H J C M and vanGemert M J C 1996 Photodynamic therapy with pulsed light sources: a theoretical analysis *Phys. Med. Biol.* **41** 835–49

Stylli S S and Kaye A H 2006 Photodynamic therapy of cerebral glioma—a review. Part II. Clinical studies *J. Clin. Neurosci.* **13** 709–17

Synytsya A, Kral V, Matejka P, Pouckova P, Volka K and Sessler J L 2004 Biodistribution assessment of a lutetium(III) texaphyrin analogue in tumor-bearing mice using NIR Fourier-transform Raman spectroscopy *Photochem. Photobiol.* **79** 453–60

Tang H M, Hamblin M R and Yow C M 2007 A comparative *in vitro* photoinactivation study of clinical isolates of multidrug-resistant pathogens *J. Infect. Chemother.* **13** 87–91

Thompson M S, Johansson A, Johansson T, Andersson-Engels S, Svanberg S, Bendsoe N and Svanberg K 2005 Clinical system for interstitial photodynamic therapy with combined on-line dosimetry measurements *Appl. Opt.* **44** 4023–31

Trachtenberg J *et al* 2007 Vascular targeted photodynamic therapy with palladium-bacteriopheophorbide photosensitizer for recurrent prostate cancer following definitive radiation therapy: assessment of safety and treatment response *J. Urol.* **178** 1974–9

Tromberg B J, Orenstein A, Kimel S, Barker S J, Hyatt J, Nelson J S and Berns M W 1990 *In vivo* tumor oxygen-tension measurements for the evaluation of the efficiency of photodynamic therapy *Photochem. Photobiol.* **52** 375–85

Tschen E H, Wong D S, Pariser D M, Dunlap F E, Houlihan A and Ferdon M B 2006 Photodynamic therapy using aminolaevulinic acid for patients with nonhyperkeratotic actinic keratoses of the face and scalp: phase IV multicentre clinical trial with 12-month follow up *Br. J. Dermatol.* **155** 1262–9

Usuda J *et al* 2006 Photodynamic therapy (PDT) for lung cancers *J. Thorac. Oncol.* **1** 489–93

Van Dyk J 1999 Radiation oncology overview *The Modern Technology of Radiation Oncology* ed J van Dyk (Madison, WI: Medical Physics Publishing) pp 1–17

van Staveren H J, Marijnissen H P A, Aalders M C G and Star W M 1995 Construction, quality assurance and calibration of spherical isotropic fibre optic light diffusers *Lasers Med. Sci.* **10** 137–47

van Staveren H J, Moes C J M, Vanmarle J, Prahl S A and vanGemert M J C 1991 Light scattering in Intralipid-10-percent in the wavelength range of 400–1100 nm *Appl. Opt.* **30** 4507–14

van Veen R L P, Robinson D J, Siersema P D and Sterenborg H J C M 2006 The importance of *in situ* dosimetry during photodynamic therapy of Barrett's esophagus *Gastrointest. Endosc.* **64** 786–8

Veenhuizen R B and Stewart F A 1995 The importance of fluence rate in photodynamic therapy—is there a parallel with ionizing-radiation dose-rate effects *Radiother. Oncol.* **37** 131–5

Vesselov L, Whittington W and Lilge L 2005 Design and performance of thin cylindrical diffusers created in Ge-doped multimode optical fibers *Appl. Opt.* **44** 2754–8

Wang I, Andersson-Engels S, Nilsson G E, Wardell K and Svanberg K 1997 Superficial blood flow following photodynamic therapy of malignant non-melanoma skin tumours measured by laser Doppler perfusion imaging *Br. J. Dermatol.* **136** 184–9

Wang L H, Jacques S L and Zheng L Q 1995 MCML—Monte-Carlo modeling of light transport in multilayered tissues *Comput. Methods Programs Biomed.* **47** 131–46

Wang K K H, Mitra S and Foster T H 2007 A comprehensive mathematical model of microscopic dose deposition in photodynamic therapy *Med. Phys.* **34** 282–93

Weersink R A, Bogaards A, Gertner M, Davidson S R H, Zhang K, Netchev G, Trachtenberg J and Wilson B C 2005 Techniques for delivery and monitoring of TOOKAD (WST09)-mediated photodynamic therapy of the prostate: clinical experience and practicalities *J. Photochem. Photobiol.* **79** 211–22

Weersink R A, Hayward J E, Diamond K R and Patterson M S 1997 Accuracy of noninvasive *in vivo* measurements of photosensitizer uptake based on a diffusion model of reflectance spectroscopy *Photochem. Photobiol.* **66** 326–35

Weishaupt K R, Gomer C J and Dougherty T J 1976 Identification of singlet oxygen as cytotoxic agent in photo-inactivation of a murine tumor *Cancer Res.* **36** 2326–9

Weissleder R, Tung C H, Mahmood U and Bogdanov A 1999 *In vivo* imaging of tumors with protease-activated near-infrared fluorescent probes *Nat. Biotechnol.* **17** 375–8

Wilson M 2004 Lethal photosensitisation of oral bacteria and its potential application in the photodynamic therapy of oral infections *Photochem. Photobiol. Sci.* **3** 412–8

Wilson B C 2006 Photonic and non photonic-based nanoparticles for cancer imaging and therapeutics *Photon Based Nanoscience and Nanobiotechnology* ed J Dubowski and S Tanev (Netherlands: Springer) pp 121–51

Wilson B C and Patterson M S 1986 The physics of photodynamic therapy *Phys. Med. Biol.* **31** 327–60

Wilson B C, Patterson M S and Lilge L 1997 Implicit and explicit dosimetry in photodynamic therapy: a new paradigm *Lasers Med. Sci.* **12** 182–99

Wilson B C and Vanlier J E 1989 Radiolabeled photosensitizers for tumor imaging and photodynamic therapy *J. Photochem. Photobiol.* **3** 459–63

Woodhams J H, Kunz L, Bown S G and MacRobert A J 2004 Correlation of real-time haemoglobin oxygen saturation monitoring during photodynamic therapy with microvascular effects and tissue necrosis in normal rat liver *Br. J. Cancer* **91** 788–94

Xu M and Alfano R R 2005 Fractal mechanisms of light scattering in biological tissue and cells *Opt. Lett.* **30** 3051–3

Xu H P and Patterson M S 2006 Application of the modified spherical harmonics method to some problems in biomedical optics *Phys. Med. Biol.* **51** N247–51

Yamamoto J *et al* 2006 Monitoring of singlet oxygen is useful for predicting the photodynamic effects in the treatment for experimental glioma *Clin. Cancer Res.* **12** 7132–9

Yu C, Canteenwala T, El Khouly M E, Araki Y, Pritzker K, Ito O, Wilson B C and Chiang L Y 2005a Efficiency of singlet oxygen production from self-assembled nanospheres of molecular micelle-like photosensitizers FC4S *J. Mater. Chem.* **15** 1857–64

Yu G Q, Durduran T, Zhou C, Wang H W, Putt M E, Saunders H M, Sehgal C M, Glatstein E, Yodh A G and Busch T M 2005b Noninvasive monitoring of murine tumor blood flow during and after photodynamic therapy provides early assessment of therapeutic efficacy *Clin. Cancer Res.* **11** 3543–52

Yu G, Durduran T, Zhou C, Zhu T C, Finlay J C, Busch T M, Malkowicz S B, Hahn S M and Yodh A G 2006 Real-time *in situ* monitoring of human prostate photodynamic therapy with diffuse light *Photochem. Photobiol.* **82** 1279–84

Yuan J, Mahama-Relue P A, Fournier R L and Hampton J A 1997 Predictions of mathematical models of tissue oxygenation and generation of singlet oxygen during photodynamic therapy *Radiat. Res.* **148** 386–94

Zelickson B, Counters J, Coles C and Selim M 2005 Light patch: preliminary report of a novel form of blue light delivery for the treatment of actinic keratosis *Dermatol. Surg.* **31** 375–8

Zeng H S, Korbelik M, Mclean D I, MacAulay C and Lui H 2002 Monitoring photoproduct formation and photobleaching by fluorescence spectroscopy has the potential to improve PDT dosimetry with a verteporfin-like photosensitizer *Photochem. Photobiol.* **75** 398–405

Zheng G, Chen J, Stefflova K, Jarvi M, Li H and Wilson B C 2007 Photodynamic molecular beacon as an activatable photosensitizer based on protease-controlled singlet oxygen quenching and activation *Proc. Natl Acad. Sci. USA* **104** 8989–94

Zhou X D, Pogue B W, Chen B, Demidenko E, Joshi R, Hoopes J and Hasan T 2006 Pretreatment photosensitizer dosimetry reduces variation in tumor response *Int. J. Radiat. Oncol. Biol. Phys.* **64** 1211–20

Zhu T C, Finlay J C and Hahn S M 2005 Determination of the distribution of light, optical properties, drug concentration, and tissue oxygenation *in-vivo* in human prostate during motexafin lutetium-mediated photodynamic therapy *J. Photochem. Photobiol.* **79** 231–41